UCRL 10253

cy 2

University of California

Ernest O. Lawrence Radiation Laboratory

SCATTERING OF NEGATIVE PIONS ON PROTONS AT 310 MeV: RECOIL-NUCLEON POLARIZATION AND PHASE-SHIFT ANALYSIS

TWO-WEEK LOAN COPY

This is a Library Circulating Copy which may be borrowed for two weeks. For a personal retention copy, call Tech. Info. Division, Ext. 5545

UCRL 10253 cy 2

DISCLAIMER

This document was prepared as an account of work sponsored by the United States Government. While this document is believed to contain correct information, neither the United States Government nor any agency thereof, nor the Regents of the University of California, nor any of their employees, makes any warranty, express or implied, or assumes any legal responsibility for the accuracy, completeness, or usefulness of any information, apparatus, product, or process disclosed, or represents that its use would not infringe privately owned rights. Reference herein to any specific commercial product, process, or service by its trade name, trademark, manufacturer, or otherwise, does not necessarily constitute or imply its endorsement, recommendation, or favoring by the United States Government or any agency thereof, or the Regents of the University of California. The views and opinions of authors expressed herein do not necessarily state or reflect those of the United States Government or any agency thereof or the Regents of the University of California.

UCRL-10253
UC-34 Physics
TID-4500 (17th Ed.)

cy 2

UNIVERSITY OF CALIFORNIA
Lawrence Radiation Laboratory
Berkeley, California

Contract No. W-7405-eng-48

SCATTERING OF NEGATIVE PIONS ON PROTONS AT 310 MeV: RECOIL-NUCLEON POLARIZATION AND PHASE-SHIFT ANALYSIS

Olav T. Vik

(Ph.D. Thesis)

May 21, 1962

SEP 1962

Printed in USA. Price $1.75. Available from the
Office of Technical Services
U. S. Department of Commerce
Washington 25, D.C.

SCATTERING OF NEGATIVE PIONS ON PROTONS AT 310 MeV: RECOIL-NUCLEON POLARIZATION AND PHASE-SHIFT ANALYSIS

Contents

Abstract v

I. Introduction 1

II. Theoretical Background 3

A. Relation of Polarization to Scattering Amplitudes . . 3

B. Scattering Amplitudes

1. Non-Spin-Flip and Spin-Flip Scattering Amplitudes 6

2. Isotopic Spin 7

C. Inclusion of Coulomb Corrections 7

D. Phase-Shift Notation 12

III. Polarization Measurements 13

A. Negative Pion Beam

1. Design 13

2. Beam Characteristics 13

B. Methods and Apparatus

1. Method 15

2. Apparatus 18

3. Counters and Electronics 18

C. Experimental Procedures

1. General 22

2. Asymmetry Measurement 23

3. Calibration 28

D. Polarization Results and Experimental Uncertainties

1. Results 29

2. Uncertainties 29

IV. Phase-Shift Analysis 32

A. Description of the Search Program 32

B. PIPANAL 1CF4 33

1. Experimental Quantities Fitted 33

2. Variation of Quantities 34
3. Error Routine 35
C. Phase-Shift Investigations 36
1. spd analysis 36
2. spdf analysis 44
3. Error analysis 46
4. Inelastic parameters 48
V. Discussion of Results 52
A. General 52
B. Comparison with theoretical predictions 53
1. p waves 53
2. d waves 53
3. f waves 55
C. Conclusions 55
Acknowledgments 56
Appendices
A. Additional Equations used in PIPANAL 57
1. π^+-p Inelastic Cross Section 57
2. π^--p Inelastic Cross Section 58
B. Error Routine Discussion and Error Matrices . . . 58
1. Calculation of Partial Derivatives . . . 58
2. Use of the Error Matrix 60
3. Error Matrices for the Aforementioned Solutions 60

SCATTERING OF NEGATIVE PIONS ON PROTONS AT 310 MeV: RECOIL-NUCLEON POLARIZATION AND PHASE-SHIFT ANALYSIS

Olav T. Vik
(Ph.D. Thesis)

Lawrence Radiation Laboratory
University of California
Berkeley, California

May 21, 1962

ABSTRACT

The recoil-proton polarization in π^--p elastic scattering at 310 MeV has been measured in the angular region 114 deg $< \theta_{c.m.} <$ 146 deg. These data have been incorporated with other polarization and differential cross-section data at this energy, and a phase-shift analysis has been performed.

Recoil-proton polarization was measured at four angles with results: 0.784 ± 0.132 at 114.2 deg, 0.648 ± 0.076 at 124.5 deg, 0.589 ± 0.072 at 133.8 deg, and 0.304 ± 0.055 at 145.2 deg. A beam of 3×10^6 pions/sec was incident on a liquid hydrogen target; the resultant recoil protons were then scattered from a carbon target and the left-right asymmetry measured. Plastic scintillation counters were used throughout.

An IBM 7090 search program was developed, and the above data were incorporated with data on π^+-p polarization and differential and total cross section, π^--p differential and total cross section, and charge-exchange differential cross section. A phase-shift analysis was performed.

Analysis for spd waves (up to $\ell = 2$) shows the existence of a single satisfactory solution to all the available data. This solution is of the Fermi type in the $I = 3/2$ phase shifts, and its $I = 1/2$ phase shifts are all small (< 6 deg), with the exception of the $D^{5/2}$ shift, which is $\approx$ 15 deg. Errors on the phase shifts vary from 0.4 through 1.1 deg.

Extension of the analysis to spdf waves ($\ell = 3$), allows three satisfactory solutions, one of which is an extension of the spd solution.

The other two solutions are also of the Fermi type with $I = 3/2$ phase shifts, but the dominant $I = 1/2$ phase shift is the $P^{1/2}$ shift, which is > 20 deg in both cases. The phase-shift errors are larger for these three solutions, ranging up to 2 deg.

The single spd solution and the three spdf solutions are discussed and compared with theoretical predictions.

I. INTRODUCTION

In the past several years increasing interest has centered about the pion-nucleon interaction. Since nuclear forces are believed to be due to the interchange of pions, the problem of their interactions with nucleons is of basic importance.

Of the pion-nucleon interactions, the most readily accessible for experiment are those involving charged pion beams and hydrogen targets. A great deal of scattering data on $\pi^{\pm}$-p reactions has been amassed over the past ten years as the starting point for theories about the pion-nucleon interactions.

Pion-nucleon scattering data can be analyzed in terms of partial waves. This involves the decomposition of scattering amplitudes into a series of terms, each term being the partial wave corresponding to a particular orbital-angular-momentum state. The presence of nucleon spin in the pion-nucleon system causes each orbital-angular-momentum state to be split into two substates corresponding to total angular momentum $J = \ell \pm 1/2$, where ℓ is the orbital-angular-momentum quantum number.

The quantities known as phase shifts are measures of the magnitude of the interaction occurring in a particular angular momentum state. They are related through the scattering amplitudes to the experimentally measurable quantities, i.e., differential cross section and recoil nucleon polarization. Any theory of the pion-nucleon interaction must be able to predict the behavior of these phase shifts; therefore, an experimental determination of the phase shifts forms a significant check on any proposed theory.

The experiment discussed in this report is a measurement of the polarization of the recoil proton in π^--p elastic scattering at 310 MeV. (In this report, the energies mentioned will refer to incident-pion kinetic energies). It is one in a series of experiments aimed at a complete and unambiguous determination of the pion-nucleon phase shifts at this energy.

A very accurate determination of π^+-p recoil-proton polarization and differential cross section has recently been carried out by Foote

et al.[1] and Rogers et al.,[2] and a comprehensive phase-shift analysis by the same authors[3] has yielded considerable information about the phase shifts for the isotopic spin $I = 3/2$ pion-nucleon system. There do exist π^--p differential cross-section and recoil-proton polarization data at 307 MeV, as reported by Zinov et al.,[4] and Vasilevskii and Vishnyakov;[5] however, the experimental errors in this data are sufficiently large to preclude an accurate phase-shift determination for the isotopic spin $I = 1/2$ pion-nucleon system. For this reason, a program was launched to measure, to the accuracy attained by Foote,[1] and Rogers,[2] the differential cross section and recoil proton polarization for π^--p elastic scattering at 310 MeV.

An intense negative-pion beam (3×10^6 π^-/sec) was developed at the 184-inch synchrocyclotron. This was scattered from a liquid hydrogen target, and the resulting recoil protons were analyzed by scattering from a carbon target. Plastic scintillation counters were used throughout to detect the particles. Simultaneous with the polarization measurement, an accurate differential cross-section measurement was carried out by Rugge.[6] The data from these two experiments was combined with those of Foote and Rogers, and a phase-shift analysis was performed.

In order to perform a phase-shift analysis, the infinite series representing the scattering amplitudes must be terminated after a finite number of terms. This number of terms will increase with increasing pion energy; this can be seen classically by considering that, as pion energy increases, higher values of angular momentum can lie within the range of the nuclear force.

At a pion energy of 310 MeV, s and p waves ($\ell = 0$ and 1) are certain to contribute, with a possibility of the appearance of d waves ($\ell = 2$). The phase-shift analysis here described included, at first, s, p, and d waves. When it was observed that the only satisfactory spd solution included a rather large d-wave phase shift, the analysis was extended to include f waves ($\ell = 3$). The results of this analysis, as well as the details concerning the recoil-proton polarization measurements, are discussed in this report.

II. THEORETICAL BACKGROUND

This section outlines the connection between the observable quantities measured and the phase shifts for the pion-nucleon system. Since confusion often arises over the definition of unit vectors in polarization measurments, an effort is made in the first subsection to specify the pertinent conventions. The extension of the usual phase-shift equations to systems of π^--p and π^0-n is reviewed, and finally the equations including nonrelativistic Coulomb and first-order relativistic Coulomb corrections are presented.

A. Relation of Polarization to Scattering Amplitudes

The notation used in this section is essentially that used by Bethe and Morrison.[7] The scattered wave function is related to the incident wave function through the scattering matrix M:

$$\psi_{\text{scattering}} = M\,\psi_{\text{incident}},$$

where $M = g(\theta) + h(\theta)\,\vec{\sigma}\cdot\hat{n}$ for a spin 1/2 particle incident on a spin 0 particle. The $\vec{\sigma}$ is the Pauli spin matrix, and the unit vector $\hat{n}$ is defined by

$$\hat{n} = \vec{k}_{\text{inc}} \times \vec{k}_{\text{scatt}} / |\vec{k}_{\text{inc}} \times \vec{k}_{\text{scatt}}|, \tag{2.1}$$

(from which it may be seen that $\hat{n}$ is perpendicular to the scattering plane).

The quantities $g(\theta)$ and $h(\theta)$ are the non-spin-flip and spin-flip scattering amplitudes that are discussed further in Sec. II.B. The differential cross section (hereafter referred to as DCS) is expressed by

$$\frac{d\sigma(\theta)}{d\Omega} = |g(\theta)|^2 + |h(\theta)|^2 \quad . \tag{2.2}$$

The expression for polarization of a spin 1/2 particle (proton) scattered from a spin 0 particle (pion) is given by[7]

$$\vec{P}(\theta) = \frac{2\mathrm{Re}\, g^*(\theta)\, h(\theta)}{|g(\theta)|^2 + |h(\theta)|^2}\, \hat{n} = P(\theta)\, \hat{n} \quad . \tag{2.3}$$

In order to measure the polarization of a given beam of particles, one may utilize scattering from a spin 0 material, in our case carbon. The DCS for scattering of a beam of particles of polarization P_1 directed along some unit vector $\hat{n}_1$ is given by

$$\frac{d\sigma}{d\Omega}(\theta) = (\,|g(\theta)|^2 + |h(\theta)|^2)[1 + P_1 P_2(\theta)\, \hat{n}_1 \cdot \hat{n}_2], \tag{2.4}$$

where P_2 and $\hat{n}_2$ are as defined by Eqs. (2.3) and (2.1).

If the scattering is in the plane perpendicular to the unit vector $\hat{n}_1$, then the quantity $\hat{n}_1 \cdot \hat{n}_2$ is $\pm$ 1. Also, we have the quantity

$$\text{Asymmetry} \equiv e(\theta) \equiv \frac{I_L(\theta) - I_R(\theta)}{I_L(\theta) + I_R(\theta)} \quad , \tag{2.5}$$

where $I_L(\theta) = \mathrm{DCS}(\theta,\, n_1 \cdot n_2 = 1)$ and $I_R(\theta) = \mathrm{DCS}(\theta,\, n_1 \cdot n_2 = -1)$. When Eq (2.4) is used, Eq. (2.5) reduces to

$$e(\theta) = P_1 P_2(\theta). \tag{2.6}$$

Equation (2.6) represents the asymmetry observable after two consecutive scatterings in the same plane, as shown in Fig. 1(a). Although the recoil proton scattering angle θ_1 is to the right, the pion scatters to the left, and hence unit vector $\hat{n}_1$ is directed out of the paper, as is unit vector $\hat{n}_2$ for θ_2 left. It should also be noted that although the proton appears to scatter right in Fig. 1(a), the center-of-mass picture shown in Fig. 1(b) indicates that both pion and proton undergo a left scattering.

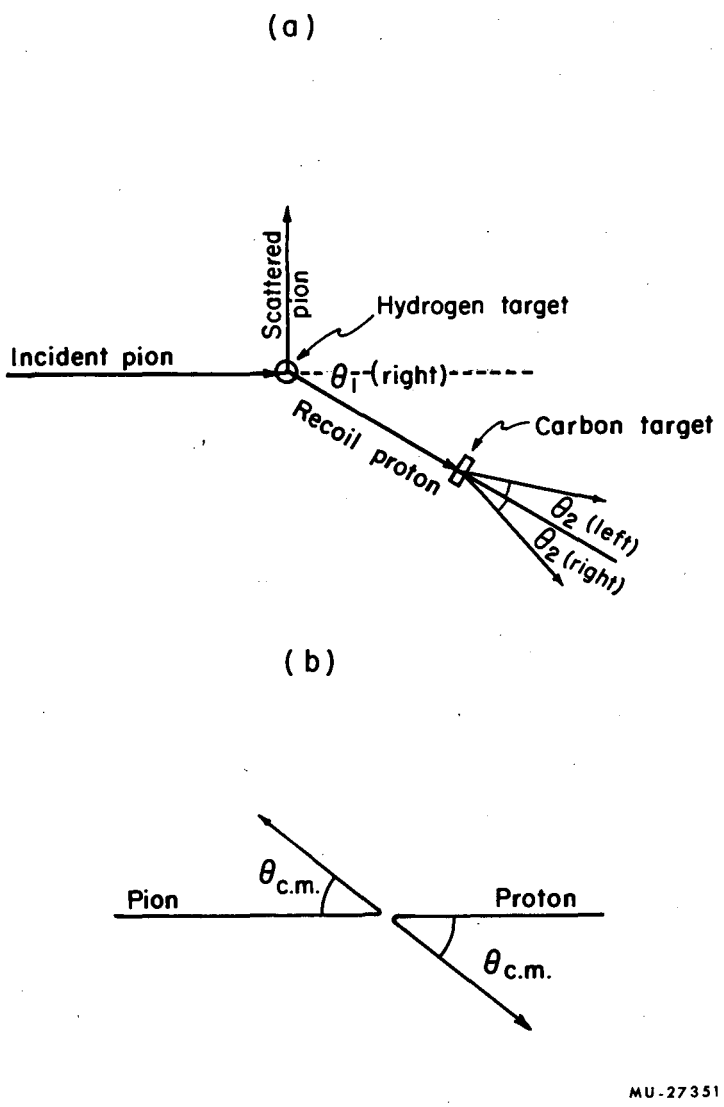

Fig. 1. (a) Scattering geometry defined in conjunction with Eq. (2.6). (b) Center-of-mass scattering geometry.

B. Scattering Amplitudes

1. Non-Spin-Flip and Spin-Flip Amplitudes

The derivation of the partial-wave expansions of the scattering amplitudes is carried out in many references, as for example, Ashkin.[8] Neglecting Coulomb effects, the result for the non-spin-flip amplitude is

$$g(\theta) = \lambda\!\!\!^{-} \sum_{\ell=0}^{\ell_{max}} \left[(\ell+1) \frac{\eta_\ell^{+}\exp[2i\delta_\ell^{+}] - 1}{2i} + \ell \frac{\eta_\ell^{-}\exp[2i\delta_\ell^{-}] - 1}{2i} \right] P_\ell(\cos\theta) \tag{2.7}$$

and the spin-flip amplitude is

$$h(\theta) = \lambda\!\!\!^{-} \sum_{\ell=1}^{\ell_{max}} \left[\frac{\eta_\ell^{+}\exp[2i\delta_\ell^{+}] - \eta_\ell^{-}\exp[2i\delta_\ell^{-}]}{2} \right] P_\ell^{1}(\cos\theta) . \tag{2.8}$$

Definitions of quantities appearing in Eqs. (2.7) and (2.8) are:

ℓ = orbital-angular-momentum quantum number.

$\delta_\ell^{\pm}$ = phase shifts for orbital-angular-momentum state ℓ and total-angular-momentum quantum number $J = \ell \pm 1/2$.

$\eta_\ell^{\pm}$ = inelastic parameters corresponding to each of the phase shifts. These are ≤ 1, being equal to unity in the absence of inelastic scattering. The use of inelastic parameters allows the phase shift $\delta_\ell^{\pm}$ to be completely real even in the presence of inelastic scattering; in this report the term "phase shift" refers to the real part $\delta_\ell^{\pm}$.

$\lambda\!\!\!^{-}$ = wavelength of either particle in the c.m. system ($\lambda\!\!\!^{-} = 1/k$).

$P_\ell(\cos\theta)$ = Legendre polynomial.

$P_\ell^{1}(\cos\theta)$ = associate Legendre polynomial, defined by

$$P_\ell^{1}(\cos\theta) = \sin\theta \frac{d}{d(\cos\theta)} P_\ell(\cos\theta).$$

θ = c.m. scattering angle for either the pion or the proton.

2. Isotopic Spin

The π^++p system, which has a z component of isotopic spin $I_z = 3/2$, can exist only in isotopic spin state $I = 3/2$. However, the π^--p system, for which $I_z = -1/2$, is a combination of isotopic spin states $I = 3/2$ and $I = 1/2$. As shown, for example, in Bethe and de Hoffman,[9] the scattering amplitudes for the three important reactions for charged pions and protons are as shown in Table I.

Table I. Scattering amplitudes for charged pions and protons.

Reaction	Scattering amplitudes	
	Non-spin-flip	Spin-flip
(a) $\pi^+ + p \rightarrow \pi^+ + p$	$g(I=3/2)$	$h(I=3/2)$
(b) $\pi^- + p \rightarrow \pi^- + p$	$1/3\,g(I=3/2)+2/3\,g(I=1/2)$	$1/3\,h(I=3/2)+2/3\,h(I=1/2)$
(c) $\pi^- + p \rightarrow \pi^0 + n$	$\frac{\sqrt{2}}{3}[g(I=3/2) - g(I=1/2)]$	$\frac{\sqrt{2}}{3}[h(I=3/2) - h(I=1/2)]$

C. Inclusion of Coulomb Corrections

The scattering amplitudes given by Eqs. (2.7) and (2.8) have been extended to take into consideration the nonrelativistic Coulomb effects as well as the first-order relativistic Coulomb corrections. This extension was carried out by Foote[3] and is based on the work of Stapp et al,[10] Solmitz,[11] and Critchfield and Dodder.[12]

In this section we use Foote's equations 7 and 8, of Sec. B,[3] to write down Coulomb-corrected scattering amplitudes for the reactions of Table I. It will now be convenient to distinguish between phase shifts for states of isotopic spin 1/2 and 3/2. In Eqs. (2.16) through (2.21) we use the notation

$\delta_\ell^{\pm}$ = phase shift for orbital-angular-momentum quantum number ℓ, total-angular-momentum state $J = \ell \pm 1/2$, and isotopic spin state $I = 1/2$;

$\eta_\ell^{\pm}$ = inelastic parameter (defined in Sec. II. B. 1.) corresponding to the $\delta_\ell^{\pm}$ phase shift above;

$\alpha_\ell^{\pm}$ = phase shift for orbital-angular-momentum quantum number ℓ, total-angular-momentum state $J = \ell \pm 1/2$, and isotopic spin state $I = 3/2$;

$\rho_\ell^{\pm}$ = inelastic parameter corresponding to the three phase shift above.

The new quantities to be introduced in Eqs. (2.16) through (2.21) are

$$n = \frac{e^2}{hv} , \tag{2.9}$$

where v is the laboratory-system velocity of the incident pion, and

$$B = \frac{(\mu_P \beta_P \beta_\pi)/2 + (2\mu_P - 1)\beta_P^2/4}{1 + \beta_\pi \beta_P} \tag{2.10}$$

where μ_P = magnetic moment of the proton in nuclear magnetons, and β_P, β_π = c.m. velocities of the proton and pion divided by the velocity of light.

$\bar{\Phi}_\ell$ is the nonrelativistic Coulomb phase shift of order ℓ. It is equal to 0 for $\ell = 0$, and is given by

$$\bar{\Phi}_\ell = \sum_{x=1}^{\ell} \tan^{-1}\left(\frac{n}{x}\right) , \text{ for } \ell \geq 1. \tag{2.11}$$

The additional parenthetical (+, -, or 0) that appear on the phase shifts in Eqs. (2.9) through (2.12) and (2.20-2.21) is necessitated because the phase shifts used in those expressions are <u>total</u> phase shifts, differing from the nuclear shifts by a small term $\bar{\Phi}_\ell^{\pm}$, which is the complete Coulomb phase shift of order ℓ. This is explained below.

The total phase shifts are related to the nuclear shifts by

$$\alpha_\ell^{\pm}(+) = \alpha_\ell^{\pm} + \Phi_\ell^{\pm}\,, \qquad \alpha_\ell^{\pm}(0) = \alpha_\ell^{\pm} - \Phi_\ell^{\pm}/2\,,$$

$$\alpha_\ell^{\pm}(-) = \alpha_\ell^{\pm} - \Phi_\ell^{\pm}\,, \qquad \delta_\ell^{\pm}(0) = \delta_\ell^{\pm} - \Phi_\ell^{\pm}/2\,.$$

$$\delta_\ell^{\pm}(-) = \delta_\ell^{\pm} - \Phi_\ell^{\pm},$$

The complete Coulomb phase shift of order ℓ, $\Phi_\ell^{\pm}$, consists of the nonrelativistic Coulomb phase shift defined by Eq. (2.11), plus a first-order nonrelativistic correction,

$$\Phi_\ell^{\pm} = \Phi_\ell + \Delta\Phi_\ell^{\pm} \tag{2.12}$$

where the first-order nonrelativistic Coulomb term is given by

$$\Delta\Phi_0 \approx n\left[\tfrac{1}{2}(\beta_P\beta_\pi) + \tfrac{1}{4}(2\mu_P - 1)\beta_P^{\,2}/(1+\beta_\pi\beta_P)\right]; \tag{2.13}$$

$$\Delta\Phi_\ell^{\,+} \approx nB/(\ell+1) \text{ for } \ell \geq 1, \tag{2.14}$$

and

$$\Delta\Phi_\ell^{\,-} \approx -\frac{nB}{\ell}\,, \text{ for } \ell \geq 1. \tag{2.15}$$

All quantities used in Eqs. (2.13) through (2.15) are defined in conjunction with Eqs. (2.9) and (2.10).

The above Coulomb phase shifts for incident pion kinetic energy $T_\pi = 310$ MeV are given in Table II.

The Coulomb-corrected scattering amplitudes for the reactions of Table I are:

<u>Reaction (a), $\pi^+ + p \rightarrow \pi^+ + p$:</u>

$$g(\theta) = -\frac{\lambda n}{2\sin^2\theta/2}\exp\left\{-in\,\ell n[\sin^2(\theta/2)]\right\}$$

$$+\lambda\sum_{\ell=0}^{\ell_{max}}\left\{(\ell+1)\,\frac{\eta_\ell^{+}\exp[2i\alpha_\ell^{+}(+)] - \exp[2i\Phi_\ell]}{2i}\right.$$

$$\left.+\ell\,\frac{\rho_\ell^{-}\exp[2i\alpha_\ell^{-}(+)] - \exp[2i\Phi_\ell]}{2i}\,P_\ell(\cos\theta)\right\}, \tag{2.16}$$

Table II. Nonrelativistic Coulomb phase shifts, first-order relativistic corrections, and complete Coulomb phase shifts (all in degrees) for incident pion kinetic energy T = 310 MeV.

ℓ	Φ_ℓ	$\Delta\Phi_\ell^+$	$\Delta\Phi_\ell^+$	Φ_ℓ^+	Φ_ℓ^-
0	0.00	0.09	----	0.09	----
1	0.44	0.09	-0.17	0.53	0.27
2	0.66	0.06	-0.09	0.72	0.57
3	0.81	0.04	-0.06	0.95	0.75

Table III. Phase shift symbols.

ℓ	J	Phase shift symbol	
		I = 3/2	I = 1/2
0	1/2	$S_{3,1}$	$S_{1,1}$
1	1/2	$P_{3,1}$	$P_{1,1}$
1	3/2	$P_{3,3}$	$P_{1,3}$
2	3/2	$D_{3,3}$	$D_{1,3}$
2	5/2	$D_{3,5}$	$D_{1,5}$
3	5/2	$F_{3,5}$	$F_{1,5}$
3	7/2	$F_{3,7}$	$F_{1,7}$

and

$$h(\theta) = \frac{i\lambda n B \sin\theta}{2\sin^2\theta/2} + \lambda \sum_{\ell=1}^{\ell_{max}} \left[\frac{\rho_\ell^{+}\exp[2i\alpha_\ell^{+}(+)] - \rho_\ell^{-}\exp[2i\alpha_\ell^{-}(+)]}{2} \right.$$

$$\left. - inB \frac{2\ell+1}{\ell(\ell+1)} \right] P_\ell^{1}(\cos\theta). \qquad (2.17)$$

<u>Reaction (b) $\pi^- + p \rightarrow \pi^- + p$:</u>

$$g(\theta) = \frac{\lambda n}{2\sin^2\theta/2} \exp\left\{ in \ln \sin^2(\theta/2) \right\} +$$

$$+ \lambda \sum_{\ell=0}^{\ell_{max}} \left[(\ell+1) \frac{\rho_\ell^{+}\exp[2i\alpha_\ell^{+}(-)] + 2\eta_\ell^{+}\exp[2i\delta_\ell^{+}(-)]}{6i} \right.$$

$$\left. + \ell \frac{\rho_\ell^{-}\exp[2i\alpha_\ell^{-}(-) + 2\eta_\ell^{-}\exp[2i\delta_\ell^{-}(-)]}{6i} - (2\ell+1)\frac{\exp[-2i\Phi_\ell]}{2i} \right] P_\ell(\cos\theta),$$

$$(2.18)$$

and

$$h(\theta) = \frac{i\lambda n B \sin\theta}{2\sin^2\theta/2}$$

$$+ \sum_{\ell=1}^{\ell_{max}} \left[\frac{\rho_\ell^{+}\exp[2i\alpha_\ell^{+}(-)] + 2\eta_\ell^{+}\exp[2i\delta_\ell^{+}(-)] - \rho_\ell^{+}\exp[2i\alpha_\ell^{-}(-)] - 2\eta_\ell}{6} \right.$$

$$\frac{-\exp[2i\delta_\ell^{-}(\delta)]}{6}$$

$$\left. + inB \left(\frac{2\ell+1}{\ell(\ell+1)} \right) \right] P_\ell^{1}(\cos\theta) . \qquad (2.19)$$

Reaction (c), $\pi^- + p \rightarrow \pi^0 + n$:

In this reaction, the incoming particles are charged and the outgoing particles are neutral. One may therefore, to the accuracy desired in this analysis, consider the Coulomb perturbation to be half as great as in reaction (b). Hence, when we use the proper isotopic spin decomposition shown in Table I, the scattering amplitudes are given by

$$g(\theta) = \frac{\sqrt{2}}{3} \lambda\!\!\!^{-} \sum_{\ell=0}^{\ell_{max}} \left[(\ell+1) \frac{\rho_\ell^+ \exp[2i\alpha_\ell^+(0)] - \eta_\ell^+ \exp[2i\delta_\ell^+(0)]}{2i} \right.$$

$$\left. + \ell \frac{\rho_\ell^- \exp[2i\alpha_\ell^-(0)] - \eta_\ell^- \exp[2i\alpha_\ell^-(0)]}{2i} \right] P_\ell(\cos\theta) \qquad (2.20)$$

and

$$h(\theta) = \frac{\sqrt{2}}{3} \lambda\!\!\!^{-} \sum_{\ell=1}^{\ell_{max}} \left[\frac{\rho_\ell^+ \exp[2i\alpha_\ell^+(0)] - \eta_\ell^+ \exp[2i\delta_\ell^+(0)] - \rho_\ell^- \exp[2i\alpha_\ell^-(0)]}{2} \right.$$

$$\left. \frac{+ \eta_\ell^- \exp[2i\delta_\ell^-(0)]}{2} \right] P_\ell^1(\cos\theta). \qquad (2.21)$$

D. Phase-Shift Notation

From this point on, "phase shift" will be understood to mean the nuclear part of the total phase shifts used in Eqs. (2.16) through (2.19). The notation developed by Foote for the π^+-p system ($I = 3/2$ state)[3] is extended to the $I = 3/2$ and $I = 1/2$ isotopic spin states. The symbol itself denotes the orbital-angular-momentum state (s, p, d, etc.), the first subscript denotes twice the isotopic spin, and the second subscript denotes twice the total angular momentum (i.e., $\ell_{2I,2J}$). The symbols are summarized in Table III.

III. POLARIZATION MEASUREMENTS

This section is devoted to a discussion of the experimental aspects of polarization measurement. Since a double scattering is involved, it was necessary to produce a very intense pion beam. This production is discussed in detail, together with the experimental apparatus and methods. Finally, the results are presented, and the uncertainties discussed.

A. Negative Pion Beam

1. Design

After a short preliminary run had shown that π^- beams produced by the external proton beam from the reaction $p+n \rightarrow p+p+\pi^-$ were unsatisfactory for polarization measurements, a study was made of possible internally produced pion beams in this energy region. A mechanical orbit plotter was used to trace the trajectory of the pion in the cyclotron field. Emerging from the cyclotron, the particles were focused by the internal strong-focusing doublet quadrupole Q_1 (Fig. 2) in such a way as to travel through the channel in the iron "meson wheel" in a parallel beam. This beam was then refocused by a second doublet quadrupole, Q_2 and then deflected by the 29X36-in. analyzer and focused in the experimental area.

An IBM 650 program DIPOLE was developed, which applied simple lens formulae to the two sections of the doublet quadrupoles, and thus calculated current settings. The final angle of bend was chosen at 36 deg to remove the dispersion introduced by the cyclotron field.

2. Beam Characteristics

The elements of the magnet system were placed in their calculated positions, and the flux through a 7-in.-diam argon-filled ionization chamber, placed at the final focus, was then optimized by varying the radial and azimuthal settings of the internal target as well as the

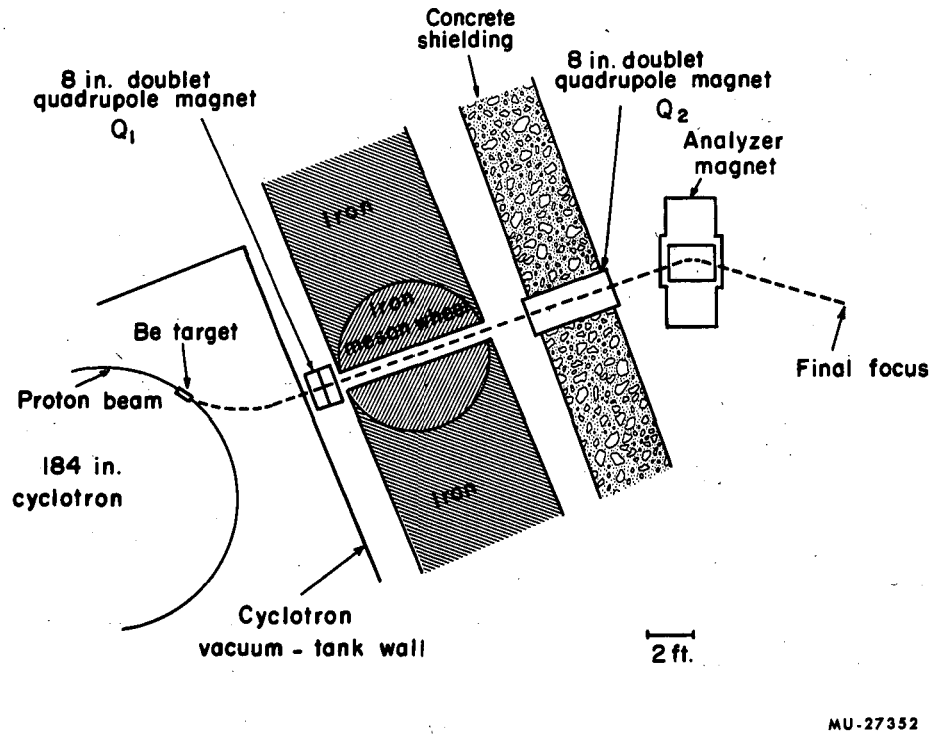

Fig. 2. Beam layout.

material of the target. The target finally used was a Be target 2 in. high, 1/2 in. radially, and 1 in. along the beam direction. Helium bags were used throughout the accessible length of the magnet system to reduce multiple scattering. The final beam had the following characteristics:

Intensity (maximum)	$3\times10^6\ \pi^-$/sec
Mean energy	310 MeV
Energy half width	5 MeV
Image full width at half max:	
Horizontal	4.2 cm
Vertical	3.2 cm
μ^- contamination	4.5%
e^- contamination	< 0.3%

It was noted that the position of the final focus was extremely sensitive to the radial setting of the internal target. The calibration of the radial target position was seen to be insufficiently accurate for the cyclotron operator to set the target properly at the start of each day's operation. For this reason it was necessary to determine the radial target position experimentally at the start of each run. This was accomplished by sweeping a pair of scintillation counters, whose defining dimensions were 1/4×1/4 in., across the beam and thus measuring the beam profile. A constant check on possible beam shifts during runs was accomplished by observing the ratio of counting rates in counters M_1 and M_2, which is discussed in the next section (III. B).

B. Methods and Apparatus

1. Method

As shown in Sec. II. A,

$$e = \frac{I_L - I_R}{I_L + I_R} = P_1 P_2, \tag{2.6}$$

where P_1 is the polarization of the beam, and P_2 is that polarization which would result from scattering an unpolarized beam through an angle θ_2. The quantity P_2 for carbon is known, so one could in principle calculate P_2 for the system; however, since our counters have finite size, and the analyzing target consists partly of carbon and partly of scintillator (see counter B, Fig. 3), we chose to determine P_2 experimentally. This is discussed in Sec. III.C.3.

The angular region measurable with a carbon analyzing target is severely limited by the sharp drop in polarization of protons on carbon below proton energies of about 120 MeV. For the largest of our proton angles (about 32 deg lab.), the energy of the recoil proton as it leaves the hydrogen target is only 130 MeV; we are therefore forced to use a thinner carbon target to minimize additional energy loss. This reduces the counting rate and makes measurement of polarization at larger angles impractical. Also, measurement of polarization at angles less than 17 deg is hindered by the main pion beam hitting the one analyzing telescope.

Referring to Fig. 3, the recoil protons were defined by a coincidence of the form ABC_1C_2. Counters A and B counted the proton, and C_1 and C_2 the scattered pion. The requirement of C_1C_2 coincidence with AB sharply reduced the possibility of counting inelastic protons, because these would not usually obey the required kinematics. The protons were then scattered by the carbon target (and also, to some extent, by counter B), and the relative intensities into counters D_1E_1 and D_2E_2 were measured. In the orientation of Fig. 3, the quantity I_L of Eq. 2.5 is given by $(ABC_1C_2D_1E_1)/ABC_1C_2$, and I_R is given by $(ABC_1C_2D_2E_2)/ABC_1C_2$.

In the interest of reducing the accidental rate, counter F was placed in anticoincidence, so that the number of triggers for counters D and E would be reduced to that number of recoil protons actually scattered out by counter B and the carbon target. The rate of $ABC_1C_2\overline{F}$ compared to ABC_1C_2 was about 12%, i.e., ≈ 12% of the protons scattered from the carbon target and counter B.

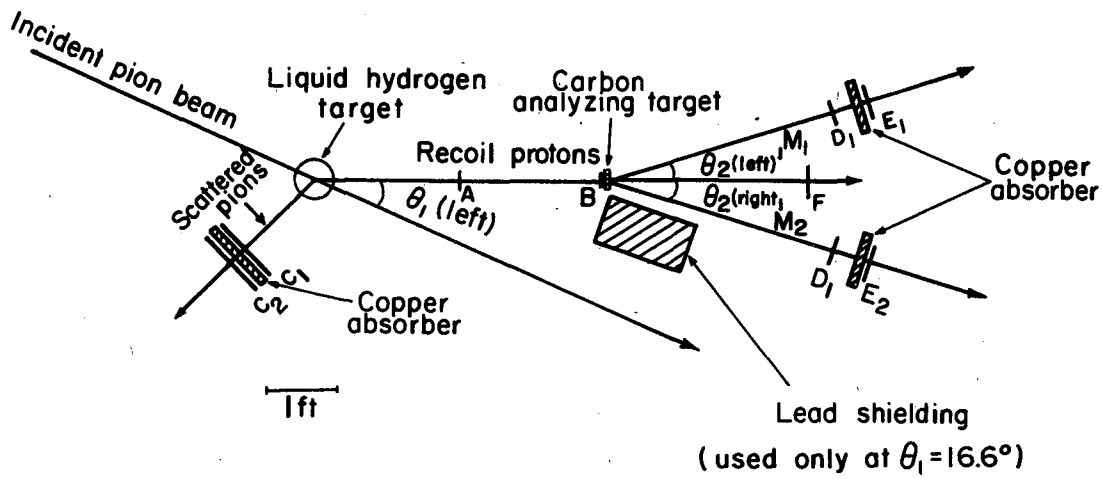

Fig. 3. Scale drawing (plan view) of counter arrangements.

Counters M_1 and M_2 were used to monitor the center line of the recoil proton beam. Counters M_1 and M_2 were moved laterally until the rates $ABC_1C_2M_1$ and $ABC_1C_2M_2$ were approximately equal. Any deviations from equality during the course of a run then indicated a shift in center line.

2. Apparatus

The liquid hydrogen target consisted of a 6-in.-diam Mylar can encased in a 12-in.-diam vacuum jacket. At beam level, the vacuum jacket consisted of 0.03-in. Mylar windows 6 in. high, supported above and below beam level by 1/2-in. Dural flanges. The Mylar extended around for 270 deg, making it possible to measure the differential cross section simultaneously with the polarization measurement. In order to measure the target-empty rate, the liquid hydrogen was forced out of the target and back into the reservoir by introducing helium gas at the top of the hydrogen container. The level of hydrogen in the target, as well as in the hydrogen reservoir, was monitored by the use of Magnehelic gauges that measured pressure differential between the top and the bottom of the target.

The scintillation counters were mounted as shown in Fig. 4. Only the scintillator parts of each counter are shown. A transit was mounted directly above the pivot as shown; the angle θ_2 was then set by sighting on the centers of counters D_1 and D_2. Counters M_1 and M_2 moved perpendicular to the beam line on a screw-driven table, which allowed setting to approximately 0.05 cm. The dimensions of the scintillators are given in Table IV.

3. Counters and Electronics

All the counters were rectangular polystyrene scintillators, connected through lucite light pipes to RCA 6810-A photomultiplier tubes.

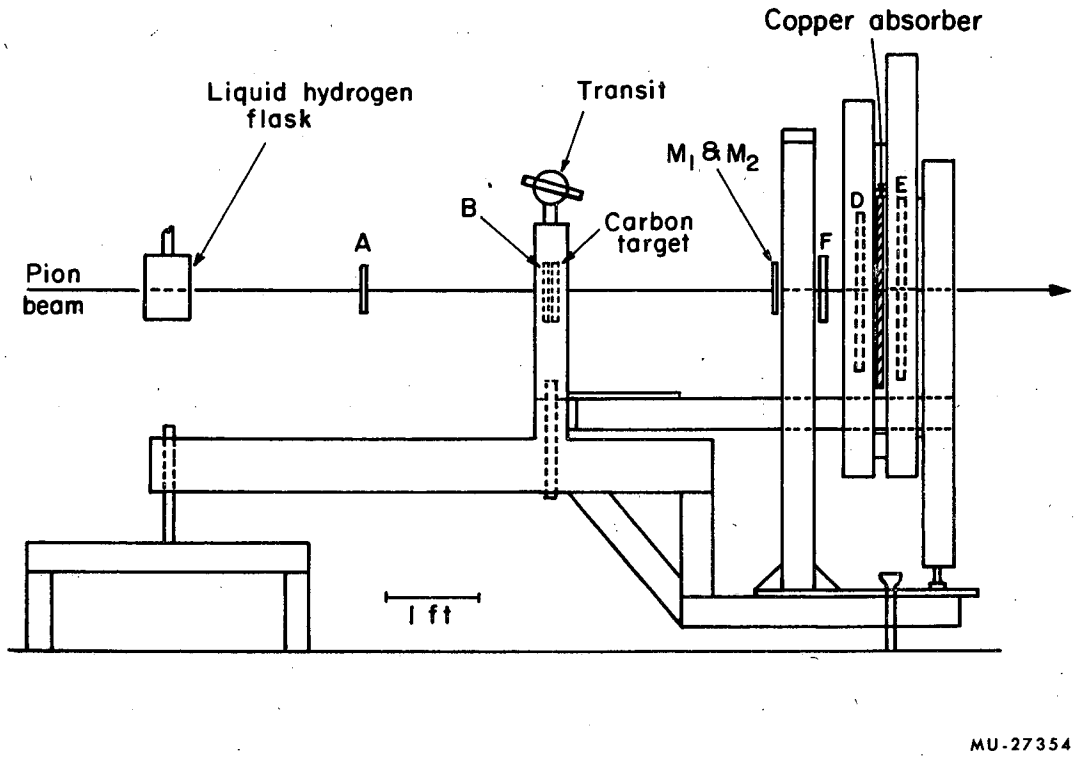

Fig. 4. Scale drawing (elevation view) of counters, including important supports (Counters C_1 and C_2 and supports are not shown).

The negative output pulse from the phototube was then amplified and fed into Wenzel coincidence circuits.[13] Attempts to form a four-fold (ABC_1C_2) coincidence proved unsuccessful, owing to the significant time spread in C_1 and C_2 pulses with respect to A and B pulses. Wherever counters of rather large dimensions were used (counters C, D, and E), it was necessary to form double coincidences of the form C_1C_2, D_1E_1, etc., and to mix the output of these doubles with the other pulses. A complete block diagram of the electronics is given in Fig. 5. The basic ABC_1C_2 coincidence was produced by two identical circuits; both these outputs were scaled, and one was used as a trigger for the remaining four types of coincidences, namely $ABC_1C_2D_1E_1\overline{F}$, $ABC_1C_2D_2E_2\overline{F}$, $ABC_1C_2M_1$, and $ABC_1C_2M_2$.

Table IV. Dimensions of counters

Counter	Dimensions (in.)
A	1/4×2×6
B	1/4×2×8
C_1 and C_2	3/8×12×12
D_1 and D_2	3/4×4×20
E_1 and E_2	3/4×6×22
F	3/4×6×12
M_1 and M_2	1/4×1×6

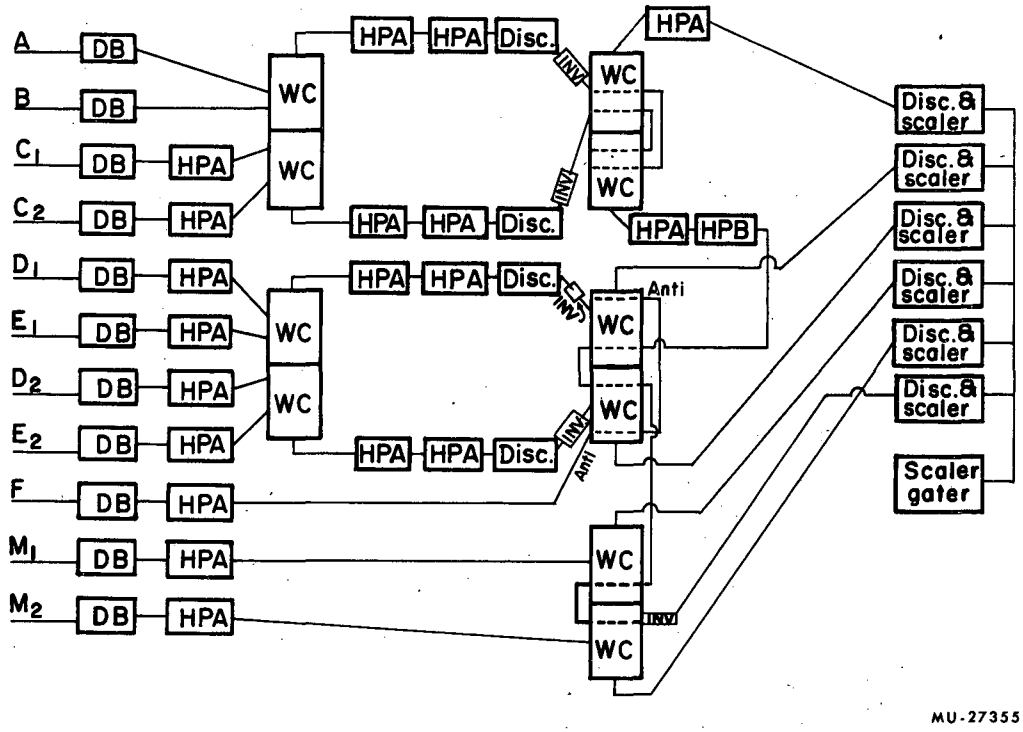

Fig. 5. Block diagram of electronics: HPA = Hewlett-Packard Model 460A amplifier; HPB = Hewlett-Packard Model 460B amplifier; DB = 125Ω variable delay box; INV = Inverter; Disc = Discriminator; WC = Wenzel-type coincidence circuit.

C. Experimental Procedures

1. General

All the counters were first placed in the pion beam and the signals properly delayed. Voltage plateaus were also determined while the counters were still in the pion beam; then the delays were adjusted to compensate for the velocity difference between pions and recoil protons.

The apparatus was then moved to an angle θ_2 of about 20 deg, and the voltage plateaus were determined for protons. Copper absorber 1/2 in. thick was placed between counters C_1 and C_2 to reduce the number of low-energy particles giving a C_1C_2 coincidence. Copper absorber was also placed between counters D and E; the amount was determined by the procedure described in Sec. III.C.2.

When the voltage levels had been determined for all counters, all voltages were changed by ±50 volts; this produced no change in counting rates. This check was repeated periodically throughout the experiment.

Accidental rates were determined by delaying counters D and E with respect to the $ABC_1C_2\overline{F}$ trigger by 52 nsec. This is the time difference between two radio-frequency fine-structure pulses of the cyclotron. The accidental counting rate was observed to be strongly dependent on the duty cycle of the cyclotron. In order to monitor the cyclotron duty cycle, the output of a scintillation counter placed in the main pion beam was displayed on an oscilloscope, and a continuous effort was made to keep the beam spread out over as long a time interval as possible.

At the smallest proton lab angle (16.9 deg) the accidental rate in the DE telescope nearest the main pion beam became prohibitive; this was improved by stacking lead between counter B and the main pion beam, thus shielding the telescope from the hydrogen target.

Possible differences in efficiency between counter telescopes D_1E_1 and D_2E_2 were minimized by reversing the positions of the two telescopes regularly; the asymmetries measured by each telescope were then compared. The asymmetry measured by each telescope at each

angle is recorded in Table V, and the final asymmetry quoted at each angle is the average of the two telescopes.

Asymmetry was measured at equal angles to the left and right of the main pion beam; since the unit vector $\hat{n}$, defined in Sec. II.B.1, is opposite in direction for these two scatterings, the preferred spin direction for a given value of polarization (P_1) also changes sign. The quantity P_2 remains the same, so the asymmetry as defined by Eq. (2.5) should also change sign. This was observed to be so, and is shown in Table V.

2. Asymmetry Measurement

Counter telescope AB was positioned at each recoil angle by means of a transit on the pion beam center line, downstream from the hydrogen target. Counter B was beam-defining, and the angle was set to about 0.05 deg. Counter telescope C_1C_2 was then set at the corresponding recoil-pion angle by means of an angle scale inscribed on the supporting table. This setting was accurate to about 0.2 deg.

The first measurement made at each recoil angle was a range determination using both counter telescopes D_1E_1 and D_2E_2. With the telescopes set at $\theta_2 = 0$ deg, the ratio $(ABC_1C_2DE)/(ABC_1C_2D)$ was measured and plotted against thickness of copper absorber between D and E. A typical range curve is shown in Fig. 6. The range determined from these curves agreed well with kinematics, and agreement between the two DE telescopes was also good.

Examination of the tail of the range curves indicated that of the real ABC_1C_2D counts, only about 2% were particles of range greater than that of protons for this recoil angle. The "set point" shown in Fig. 6 indicates the amount of copper absorber placed between counters D and E during asymmetry measurements. This absorber was used in part to discriminate against protons that scatter inelastically from carbon and in part to reduce the number of DE coincidences from stray low-energy particles. The "set point" for each recoil angle is given in Table VI.

Table V. Asymmetry summary.

θ_1 (lab) (deg)	Telescope D_1E_1	Telescope D_2E_2	Average asymmetry[a]
16.6 L	-0.092±.047[b]	-0.183±.050	-0.135±.034
16.6 R	0.235±.067	0.143±.050	0.177±.040
22.1 L	-0.192±.049	-0.270±.044	-0.236±.033
22.1 R	0.288±.050	0.304±.050	0.296±.035
26.6 R[c]	0.366±.046	0.377±.041	0.371±.031
31.6 L	-0.295±.060	-0.193±.064	-0.248±.044
31.6 R	0.298±.088	0.330±.079	0.316±.059

[a] The average asymmetry was obtained by combining the measurements of the two telescopes weighted by the inverse of the square of their errors. The error quoted is equal to $[(\Delta e_1)^{-2} + (\Delta e_2)^{-2}]^{-1/2}$, where Δe_1 and Δe_2 are the errors on the asymmetry measured by telescopes 1 and 2.

[b] All errors quoted on this page are based on counting statistics.

[c] Time limitations made it impractical to measure the asymmetry for θ_1 = 26.6 deg L. In view of the good agreement between left and right at the other three angles it was deemed unnecessary to make the measurement at θ_1 = 26.6 deg L.

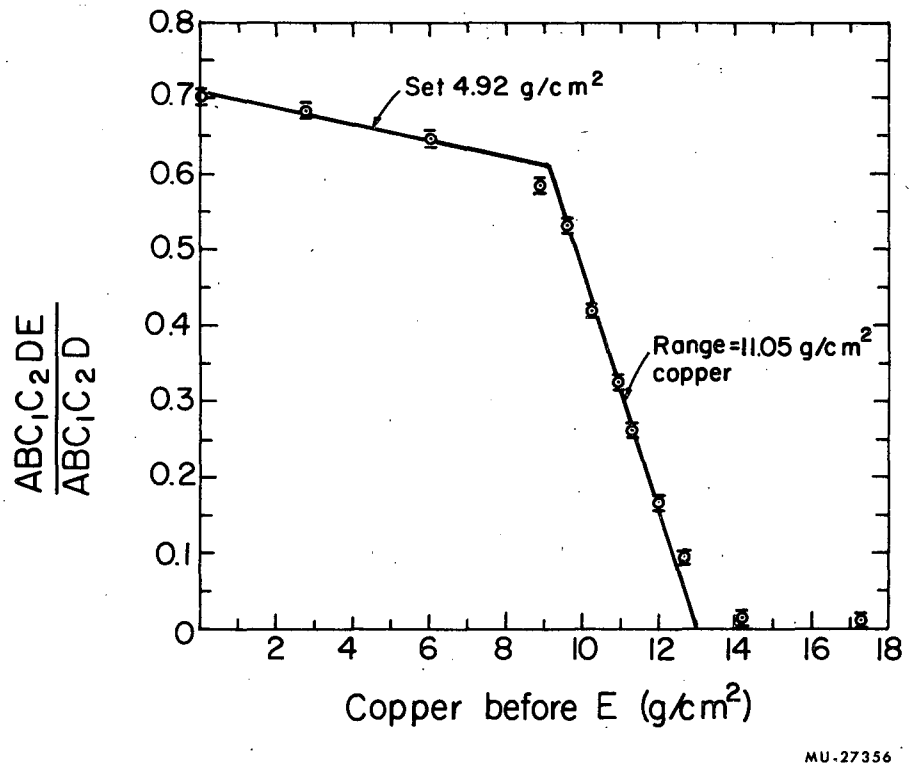

Fig. 6. Range curve on recoil protons, where θ_1 = 31.6 deg.

Table VI. Summary of pertinent quantities

Quantity	Mean recoil-proton lab angle (deg)			
	16.6	22.1	26.6	31.6
c.m. scattering angle (deg)	145.2	133.8	124.5	114.2
Analyzing-telescope angle Q_2 (deg)	15.5	15.5	17.0	17.0
Thickness of carbon-analyzing target (in.)	2.0	1.0	0.5	0.5
Copper absorber thickness between counters D and E (g/cm^2)	5.03	7.90	6.42	4.29
Approx scattered-proton rate (ABC_1C_2) per minute	1250	900	680	650
Approx average analyzed-proton rate ($ABC_1C_2DE\bar{F}$) per minute	3	1.3	0.7	0.9
Total number of full-normal counts recorded	2400	2200	1350	1250

The center line of the recoil-proton beam was then determined for the two telescopes. This was accomplished by sweeping each telescope across the proton beam in 1-deg steps, and plotting $(ABC_1C_2DE)/(ABC_1C_2)$ against θ_2. A proton beam profile measured in this manner is given in Fig. 7. The center line was determined to 0.05 deg. Checks were made frequently during the early stages of the experiment to ascertain the constancy of the center line. Later it was concluded that keeping the ratio $(ABC_1C_2M_1)/(ABC_1C_2M_2)$ between 0.90 and 1.10 guaranteed a shift in proton center line of less than 0.05 deg.

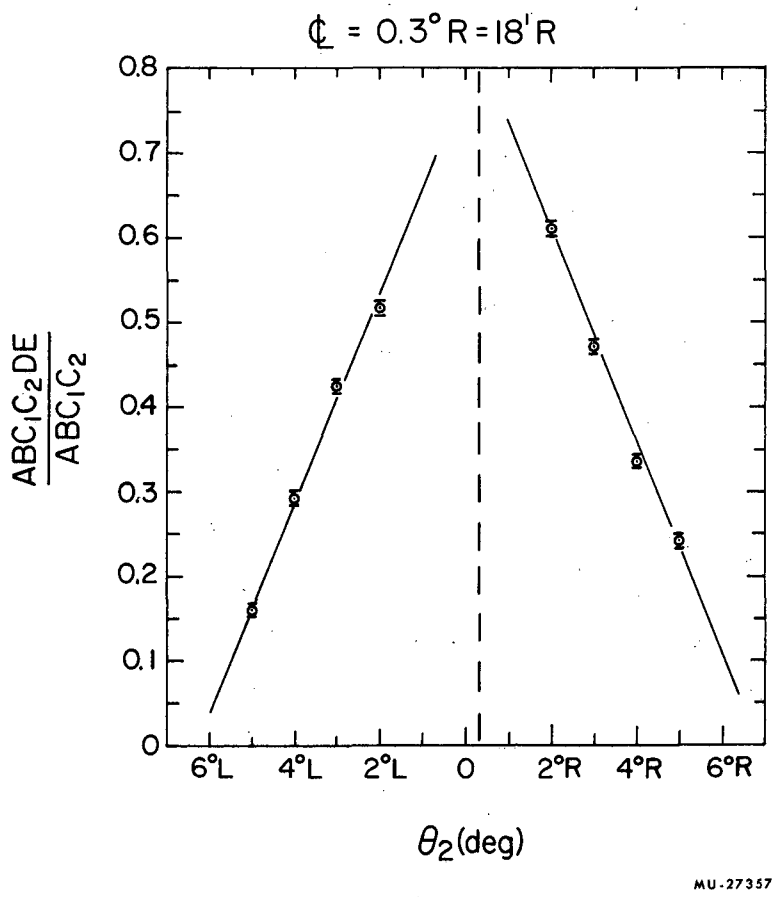

Fig. 7. Centerline curve.

Telescopes C_1D_1 and C_2D_2 were then set at equal angles θ_2 measured from the center line as determined by the respective telescope. The following four counting rates were measured:

(a) target full, delays normal;

(b) target full, DE delayed 52 nsec with respect to $ABC_1C_2\overline{F}$;

(c) target empty, delays normal; and

(d) target empty, DE delayed 52 nsec with respect to $ABC_1C_2\overline{F}$.

Rates (a) and (b) were monitored against the ABC_1C_2 rate, as well as against readings of an argon-filled ionization chamber placed in the main pion beam before the hydrogen target; rates (c) and (d) were monitored against the ionization chamber only.

At all angles, rate (c) was less than 4% of rate (a). At $\theta = 31.6$ deg, rate (b) was about 7% of rate (a), and at all other angles it was less than 5%. As a check on the validity of measuring accidentals in this manner, the beam was turned down to about 1.5×10^6 π/sec, and asymmetry was measured for $\theta = 31.6$ deg. Rate (b) dropped to less than 5%, but the net counting rates were unchanged. Rate (d) was in all cases less than 1%.

Table VI summarizes pertinent quantities for each of the angles measured.

3. Calibration

As mentioned in Sec. III.B.1., the quantity P_2 was determined experimentally for this counter arrangement. This calibration was carried out by Foote,[1] and will be discussed very briefly here. The reader is referred to the above publication for a detailed account of the calibration procedure.

A beam of protons was scattered from a 1/2-in. carbon target at an angle of 13.8 deg. These scattered protons were then analyzed by the counter system under conditions identical with that of the actual asymmetry measurements, as discussed in Section III.C.2. This measured quantity e_2 is then equal to P_1P_2, where P_1 is the polarization of the once-scattered proton beam. P_1 was calculated from data of

Dickson and Salter,[14] Tyren et al.,[15] and Hafner.[16] The values of $P_2 = e_2/P_1$ quoted in Table VII are the averaged values given in Foote.[1]

D. Polarization Results and Experimental Uncertainties

1. Results

Table VI presents the measured asymmetries as determined by the two telescopes for θ_1 to the left and right. The results from the two telescopes are averaged, and the values for θ_1 left and right are in turn averaged and listed in Table VII.

2. Uncertainties

The principal sources of error in the asymmetry measurements are due to counting statistics and uncertainty in recoil-proton beam center line. Counting statistical errors in asymmetry are related to errors in I_L and I_R (see Eq. 2.6) by[17]

$$\Delta e \approx \frac{1 - e^2}{2} \sqrt{\left(\frac{\Delta I_L}{I_L}\right)^2 + \left(\frac{\Delta I_R}{I_R}\right)^2} .$$

These errors are quoted in Table VI.

Uncertainty in asymmetry due to uncertainty in center line is related to angular uncertainty by[17]

$$\frac{de}{d\theta_2} \approx \frac{d(\ln I_0)}{d\theta_2} ,$$

where I_0 is the average DCS for scattering at a lab angle θ_2 (see Fig. 3). For the geometries used in the aforementioned experimental arrangements, $de/d\theta_2 \approx 0.2$/degree.

As was stated in Sec. III.C.2, the recoil-proton beam center line was determined to about 0.05 deg from the umbra curves. The monitor counters M_1 and M_2 guaranteed the constancy of the beam center line during the course of any run. The transit made angle settings possible to about 0.02 deg, a negligible contribution to the

Table VII. Polarization summary.

Center-of-mass angle (deg)	114.2	124.5	133.8	145.2
Average asymmetry[a]	0.269 ± .037[b]	0.371 ± .032	0.264 ± .026	0.152 ± .027
Analyzing ability[c]	0.344 ± .034	0.573 ± .046	0.449 ± .032	0.500 ± .020
Recoil-proton polarization	0.784 ± .132	0.648 ± .076	0.589 ± .072	0.304 ± .055

[a] This is the average of the two asymmetries measured by telescopes 1 and 2 given in Table V. The individual quantities have been weighted by the inverse of the square of their errors.

[b] This quoted error in asymmetry includes the uncertainty of 0.09 due to center-line uncertainty (see Sec. III. D.2.)

[c] This analyzing ability was measured by Foote[1] and is the average of the values given in Table V.

uncertainty. From these considerations, the rms error due to center line uncertainty was $e \approx 0.010$. This error was added in rms fashion to the counting statistical uncertainties, and quoted in Table VII.

The mean lab recoil-proton angle is assumed to be known to 0.40 deg. This uncertainty arises partly from uncertainty in the pion beam center line, and partly from the calculation necessary to determine the mean lab angle from the actual center line of counters A and B. (This calculation is necessitated by the variation of the DCS across the finite size of counters A and B.) The incident pion beam center line was determined to 0.3 deg, and the setting of the A-B center line by transit was good to about 0.1 deg. The pion beam was centered on the liquid hydrogen target at the beginning of each day by methods outlined in Sec. III.A.2, so that variations of beam center line from day to day were minimized.

IV. PHASE-SHIFT ANALYSIS

The polarization data presented in Sec. III were incorporated with the π^+-p polarization data of Foote,[1] the π^+-p DCS and total cross-section data of Rogers,[2] and recent π^--p DCS and total cross-section data of Rugge.[6] A phase-shift analysis has been performed; this section deals with the IBM 7090 program developed for this purpose, and the results of the phase-shift search are presented.

A. Description of the Search Program

As may be judged from Sec. II, the phase-shift expansions of the scattering amplitudes describing the π-p system are very complicated functions, and so there is no simple way of deriving values for the phase shifts from the available experimental data. Modern high-speed computer techniques make it possible, however, to calculate very rapidly the values of DCS and polarization predicted by a given set of phase shifts.

The PIPANAL program developed for this purpose, employs the grid-search method for fitting the phase-shift equations to experimental points. A tentative set of phase shifts is fed into the program, and the computer then varies all the phase shifts in turn, in order to minimize the quantity

$$M = \sum \left[\frac{Q_{calc} - Q_{exp}}{\Delta Q_{exp}} \right]^2 , \tag{4.1}$$

where Q_{calc} refers to the value of DCS or polarization calculated from a given set of phase shifts, Q_{exp} is the corresponding experimentally determined value, and ΔQ_{exp} is the experimental uncertainty in Q_{exp}. The summation is over all the experimental quantities being considered in a given case.

Each phase shift is varied in turn, and this procedure is repeated until a complete cycle results in no reduction in the value of M. The increment of change in phase shift is then reduced, and the above process is repeated until the increment reaches a certain predetermined value.

B. PIPANAL 1CF4

PIPANAL 1CF4 is based on the IBM 704 program developed by Foote,[3] and has evolved through several intermediate programs. It is the most complete program developed, and the only one discussed in this report. It is to be understood, however, that not all the analysis discussed in the following sections was performed by this program, but sometimes by less inclusive and therefore less time-consuming programs of the same type.

1. Experimental Quantities Fitted

Experimental quantities fitted by PIPANAL 1CF4 are:

(a) DCS–The program accepts up to 30 DCS points each for the three reactions given in Table I.

(b) Polarization–The program accepts up to 10 points each for the reactions in Table I.

(c) Total cross section–The program accepts a total cross section for π^+-p and π^--p scattering. Since total cross sections are usually determined experimentally between two cutoff angles, the program fits them to the numerically integrated value under the calculated DCS curve between these cutoff angles. A predetermined fraction of the calculated inelastic cross section was also added (see Eqs. A.3 and A.4 of Appendix A), and in the case of π^--p scattering, the integration was under the DCS curve for both reactions (b) and (c) of Table I.

(d) Inelastic cross section–Only the π^--p inelastic cross section was fitted, since only the I = 1/2 inelastic parameters are allowed to vary (see Sec. 2 below).

(e) Legendre coefficients for charge-exchange scattering—The commonest way of measuring the DCS for the reactions $\pi^- + p \rightarrow \pi^0 + n$ is to measure the γ-ray distribution from the decaying π^0. When this is the case, the γ-ray distribution is fitted in a Legendre expansion, and the coefficients for a Legendre expansion of the π^0 distribution are related to those of the γ distribution.[18] For this reason, data on the $\pi^- + p \rightarrow \pi^0 + n$ DCS is often quoted in terms of these Legendre coefficients. Therefore the program was equipped to fit these coefficients with coefficients calculated from the phase shifts. Up to seven Legendre coefficients can be fitted (corresponding to an spdf wave fit to the γ distribution).

2. Variation of Quantities

Quantities are varied in PIPANAL 1CF4 as follows:

(a) Phase shifts—The program varies phase shifts for $I = 1/2$ and $I = 3/2$ states. It can perform sp, spd, or spdf analysis for $\pi^{\pm}$-p systems of any energy.

(b) Inelastic parameters—In the case of π^+-p scattering, the total inelastic cross section is quite small as compared with the total elastic cross section (< 1 mb as compared with 60 mb). For this reason, the inelastic parameters $\rho_\ell^{\pm}$ (see Sec. II.B) are not varied in the search. It is possible, however, to insert $\rho_\ell^{\pm}$ different from 1 into the input data, and thus study the possible effects of inelastic parameters on the phase shifts. The inelastic cross section for π^--p scattering is, however, as large as 1.5 mb, as compared with $\approx$ 29 mb for the π^--p elastic total cross section. (In this context "elastic" refers to both $\pi^- + p \rightarrow \pi^- + p$ and $\pi^- + p \rightarrow \pi^0 + n$ reactions). We accordingly allowed the quantities $\eta_\ell^{\pm}$ to be varied in the search, with the constraint that they had to remain in the interval $0 \leq \eta_\ell^{\pm} \leq 1$. The assumption made here was that since the total inelastic cross section for π^+-p (which is all isotopic spin 3/2) is very small, the contribution to the larger π^--p inelastic cross section must be from the isotopic spin 1/2 state.

(c) Normalization parameters–In the measurement of DCS there is always an uncertainty of a few percent in the normalization of the angular distributions. In order to enable the search program to move the angular distribution up or down an amount corresponding to this uncertainty, quantities ϵ^+, ϵ^- and ϵ^0 were introduced for each of the three differential cross sections mentioned in Sec. B.1 above. Each of the experimental DCS points was multiplied by the quantity $(1+\epsilon)$ to adjust the distribution, and the contribution of DCS to Eq. (4.1) was modified to become

$$M(DCS) = \sum \left[\frac{DCS_{calc} - DCS_{exp}(1+\epsilon)}{\Delta DCS_{exp}} \right]^2 + \left(\frac{\epsilon}{\Delta\epsilon} \right)^2 , \qquad (4.2)$$

where $\Delta\epsilon$ is the experimental uncertainty in normalization.

3. Error Routine

The validity of any phase-shift solution is limited unless the error on each phase shift is known. Approximate values of the errors on the phase shifts were determined. These are quoted in Appendix B.

The method used in determining errors was the standard error-matrix approach. After the minimum value of M (Eq. 4.1) has been found, the shape of the M hypersurface near the minimum is examined by computing the second partial derivatives of M with respect to each of the phase shifts used. These partial derivatives form a matrix G defined by

$$G_{ij} = \frac{1}{2} \frac{\partial^2 M}{\partial\delta_i \partial\delta_j} .$$

This matrix is then inverted, yielding the error matrix G^{-1} with the properties

$$\sqrt{(G^{-1})_{ii}} = (\Delta\delta_i)_{rms} , \text{ and } (G^{-1})_{ij} = C_{ij} (\Delta\delta_i)_{rms} (\Delta\delta_j)_{rms} \text{ (for } i \neq j),$$

where C_{ij} is the correlation coefficient.

For details of the calculation of the elements of G, comments on the use of G^{-1}, and references, see Appendix B. Error matrices for the principal phase-shift solutions are also presented in Appendix B.

C. Phase-Shift Investigations

The general approach followed in searching for phase-shift solutions to the experimental data is the random-starting-point method. A large number of sets of random phase shifts (over the period -180 deg $\leq \delta \leq$ 180 deg) are introduced as input data, and the program is requested to find the local minimal value for M. If a sufficient number of randomly located starting points is used, the probability of having missed a "good" solution is small.

When all phase shifts are allowed to vary simultaneously (as in PIPANAL 1CF4) the process of random searching is extremely time-consuming. For this reason, the following method was used: The three (one spd and two spdf) I = 3/2 solutions of Foote[3] were taken as starting points, and were held fixed in all of the random searching. Only the DCS data of Rugge (Table VIII)[6] were fitted in this manner, and for each I = 3/2 set, there were in general several I = 1/2 sets that satisfactorily fitted the DCS data. These "good" solutions were then inserted into PIPANAL 1CF4 the π^+-p data shown in Tables IX and X were included, and all phase shifts were allowed to vary simultaneously. Polarization data were then introduced, and finally charge-exchange DCS (Caris[19]), in order to rule out some of the I = 1/2 phase-shift sets. This procedure is discussed in detail in the following two subsections.

The data used in all of the analysis following is given in Table VI through X.

1. spd Analysis

A least-squares fit of the DCS data of Rugge[6] indicated the need for at least d waves to obtain a satisfactory fit. This section deals with the details of the spd analysis.

Table VIII. Differential and total cross section[a] for $\pi^- + p \rightarrow \pi^- + p$, measured by Rugge[b]

θ_{cm} (deg)	$\frac{d\sigma(\theta)}{d\Omega_{cm}}$ (mb/sr)	rms uncertainty (mb/sr)
34.7	1.184	0.043
41.4	1.171	0.035
47.9	1.151	0.033
54.4	1.125	0.029
60.6	1.027	0.027
66.8	0.970	0.023
72.7	0.853	0.023
78.5	0.774	0.018
84.1	0.690	0.018
89.6	0.635	0.015
94.9	0.561	0.017
100.0	0.498	0.013
105.0	0.461	0.014
109.8	0.480	0.009
114.5	0.482	0.016
119.0	0.514	0.012
123.5	0.536	0.013
127.8	0.590	0.018
132.0	0.663	0.016
136.0	0.715	0.016
140.0	0.764	0.021
144.0	0.822	0.020
147.8	0.817	0.021
151.6	0.889	0.025
155.2	0.941	0.015
158.9	0.991	0.028
162.4	0.932	0.029
166.0	0.944	0.042

[a] The total cross section used in the analysis was 28.8± 0.8 mb, evaluated between cutoff angles 8.4 and 167.4 deg. The normalization uncertainty (see Sec. IV. B) was taken to be $\Delta\epsilon = 0.04$.

[b] See reference 6

Fermi 3/2 starting point. In the analysis by Foote[3] (see his Table IV), only the solution of the Fermi type is totally acceptable. The Minami solution is theoretically unsatisfactory because of the very large $D_{3,3}$ shift, and the Yang solution is highly improbable because of the large M value. We therefore concentrated our efforts on the Fermi solution (the Yang type is mentioned briefly below).

Using Foote's Fermi solution ($S_{3,1} = -18.5$; $P_{3,1} = -4.7$; $P_{3,3} = 134.8$; $D_{3,3} = 1.9$; $D_{3,5} = -4.0$) as the fixed $I = 3/2$ phase shifts, a total of 115 random sets was introduced. Four distinct solutions were found to be acceptable fits to the π^--p DCS data. These four solutions, after having been fitted with PIPANAL 1CF4, were as shown in Table XII. The π^--p recoil-proton polarization predicted by these four solutions is shown in Fig. 8. It is obvious from the figure that solutions (1) and (2) are in agreement with the data, while (3) and (4) are not. Inclusion of polarization data in the program causes solution (3) to degenerate into solution (1), while the M value of solution (4) increases to a very unacceptable 450 (where 48 is expected).

As is also clear from Fig. 8, polarization data in the region we have explored are quite incapable of resolving solutions (1) and (2). One method of resolving this ambiguity would be to obtain π^--p polarization data at smaller angles. Such data do not exist at present, but an attempt has been made to resolve the two solutions by the inclusion of $\pi^- + p \rightarrow \pi^0 + n$ DCS.[19] This procedure was suggested by the large variation in the backward direction of the predicted charge-exchange DCS curves shown in Fig. 9.

Inclusion of the coefficients of Table XI together with the polarization data of Table VII in the search program yielded the results shown in Table XIII. Evidently, only solution (1) of Table XIII now has a reasonable M value, and is therefore considered the only satisfactory spd solution to all the aforementioned data.

Yang 3/2 starting point. While the most intensive work has been centered around the Fermi solution, the Yang spd solution of Foote[3]

Table IX. Differential and total cross section[a] for $\pi^+ + p \rightarrow \pi^+ + p$, measured by Rogers.[b]

θ_{cm} (deg)	$\frac{d\sigma(\theta)}{d\Omega_{cm}}$ (mb/sr)	rms uncertainty (mb/sr)
14.0	18.71	0.60
19.6	16.05	0.46
25.2	13.82	0.31
30.6	12.99	0.25
34.6	12.28	0.27
36.2	11.65	0.27
44.0	9.82	0.15
51.8	8.59	0.26
56.8	7.54	0.28
60.0	6.58	0.22
69.6	4.73	0.10
75.3	3.62	0.09
81.6	2.77	0.08
97.8	1.66	0.07
105.0	1.51	0.06
108.1	1.62	0.07
120.9	2.08	0.08
135.2	2.93	0.14
140.6	3.36	0.12
144.7	3.76	0.15
152.2	4.10	0.21
156.4	4.51	0.17
165.0	4.88	0.12

[a] The total cross section used in the analysis was 56.4± 1.4 mb, evaluated between cutoff angles 14.7 and 158.0 deg. The normalization uncertainty (see Sec. IV.B) was taken to be $\Delta\epsilon = 0.06$.

[b] See reference 2.

Table X. Recoil-proton polarization for $\pi^+ + p \rightarrow \pi^+ + p$, measured by Foote[a]

θ_{cm} (deg)	$P(\theta)$	rms uncertainty
114.2	0.044	0.062
124.5	-0.164	0.070
133.8	-0.155	0.044
145.2	-0.162	0.037

[a]See reference 1.

Table XI. Coefficients for Legendre polynomial fit to $\pi^- + p \rightarrow \pi^0 + n$ DCS, measured by Caris[a] at 317 MeV.

$$\frac{d\sigma(\theta)}{d\Omega_{cm}} = \sum_{\ell=1}^{\ell_{max}} A_\ell P_\ell(\cos\theta)$$

	Coefficient (mb/sr)	rms uncertainty[b] (mb/sr)
A_1	1.39	0.06
A_2	1.87	0.11
A_3	1.50	0.17
A_4	0.01	0.15
A_5	-0.35	0.42

[a] See reference 19.

[b] The normalization uncertainty (see Sec. IV.B) was taken to be $\Delta\epsilon = 0.10$.

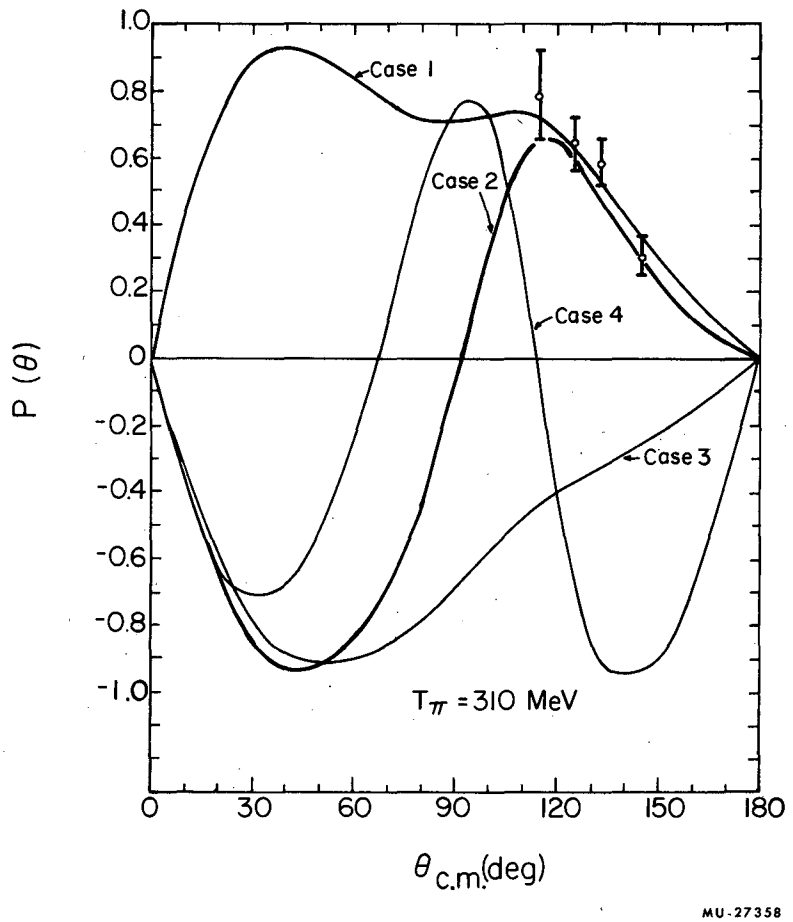

Fig. 8. Recoil-proton polarization in π^--p elastic scattering at 310 MeV. Cases plotted are those given in Table XII.

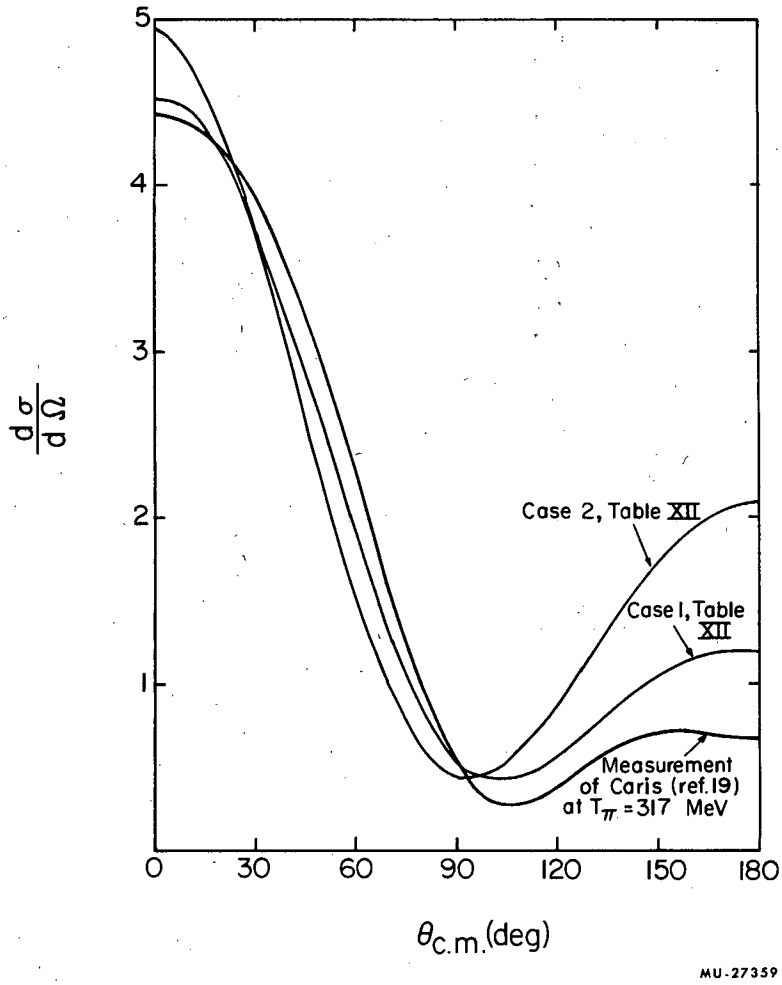

Fig. 9. Comparison between predicted and measured charge-exchange DCS.

Table XII. spd solutions to π^--p DCS and total cross-section data (also π^+-p DCS, polarization, and total cross-section data).

	$M_{expected}=47^a$	$S_{3,1}$	$P_{3,1}$	$P_{3,3}$	$D_{3,3}$	$D_{3,5}$	$S_{1,1}$	$P_{1,1}$	$P_{1,3}$	$D_{1,3}$	$D_{1,5}$
(1)	52.4	-18.8	-5.0	134.9	1.7	-3.7	-5.8	-4.0	4.4	-5.3	15.1
(2)	61.3	-18.2	-4.5	135.1	1.9	-4.0	-7.2	25.8	7.3	3.0	-0.5
(3)	57.8	-18.5	-4.7	134.7	1.9	-4.0	4.2	10.5	-2.0	3.6	-0.0
(4)	52.1	-18.9	-5.0	134.3	1.8	-3.9	-4.0	-0.6	5.3	17.3	1.0

Table XIII. spd solutions to π^--p DCS, polarization, total cross-section and charge-exchange coefficients (also π^+-p DCS, polarization, and total cross-section data)

	$M_{expected}=56^a$	$S_{3,1}$	$P_{3,1}$	$P_{3,3}$	$D_{3,3}$	$D_{3,5}$	$S_{1,1}$	$P_{1,1}$	$P_{1,3}$	$D_{1,3}$	$D_{1,5}$
(1)	71.2	-18.8	-4.9	135.5	1.7	-3.6	-6.2	-4.0	3.9	-5.5	15.2
(2)	123.4	-18.3	-4.4	135.7	1.8	-3.9	-2.6	28.7	6.7	2.8	-0.3

[a] $M_{expected}$ means the number of degrees of freedom, i.e., (number of experimental points fitted) minus (number of phase shifts varied).

is perhaps reasonable enough to merit some consideration. We therefore did a considerably smaller amount of random searching in this area also, using as fixed input 3/2 shifts: $S_{3,1} = -23.2$; $P_{3,1} = 126.2$; $P_{3,3} = 159.0$; $D_{3,3} = 7.5$; and $D_{3,5} = -4.6$. In 40 random sets, only one solution of $M \leq 50$ ($M = 23$ is expected) appeared; but this solution can be ruled out by π^--p polarization data.

2. spdf Analysis

The same general procedure was followed for the spdf analysis as for the spd analysis. In this case, the Fermi I and Fermi II spdf solutions of Foote[3] were regarded as the most important, and the remaining solutions were treated somewhat more sketchily. "Random" sets were random only in s-, p-, and d-wave phase shifts, with the f waves assumed small and started at zero deg in all cases. However, the final solutions often yielded f-wave phase shifts as large as 10 deg, leading us to believe that no great bias was introduced by starting the f-wave phase shifts at zero.

Fermi I and II. Fitting the π^--p DCS data with I = 3/2 phase shifts fixed yielded, as one might expect, a considerable number of satisfactory solutions. A total of 400 random sets was run, with a total of 23 good solutions emerging. Of these, 14 were of the Fermi I type and 9 were of the Fermi II type.

Addition of π^--p polarization reduced this number of solutions to 5; these are presented in Table XIV. Use of the five charge-exchange DCS coefficients of Caris[19] eliminated solutions (4) through (7); the remaining three are shown in Table XV, and these three solutions are sufficiently different to warrant short individual discussions:

Solution (1)—This is the spdf counterpart of the only good spd solution given in Table XII. The I = 3/2 phase shifts of the final solution agree very well with Foote's Fermi I solution.[3] Each type of data is individually fitted well. The M value is very close to the expected value; it is the most frequently occurring solution, having appeared 37 times during the random search.

Table XIV. spdf Solutions to π^+-p and π^--p DCS, polarization, and total cross section.

$M_{expected} = 47$[a]

	M	Started from	$S_{3,1}$	$P_{3,1}$	$P_{3,3}$	$D_{3,3}$	$D_{3,5}$	$F_{3,5}$	$F_{3,7}$	$S_{1,1}$	$P_{1,1}$	$P_{1,3}$	$D_{1,3}$	$D_{1,5}$	$F_{1,5}$	$F_{1,7}$
I	37.9	Fermi I	-15.3	-0.0	134.8	4.8	-6.4	0.8	-1.6	-5.4	-5.3	2.0	-5.5	15.9	-0.2	2.4
II	48.3	"	-20.7	-10.1	136.1	-2.0	-0.3	-1.1	2.3	11.7	23.4	-2.0	6.7	2.5	2.2	-0.4
III	41.3	"	-15.1	0.1	135.0	4.9	-6.4	0.8	-1.7	-0.2	27.2	7.3	-0.3	-1.6	-2.5	-0.2
IV	49.1	"	-17.4	-2.8	134.2	3.2	-5.1	0.6	-0.8	1[illegible].3	20.2	-1.2	5.3	5.7	1.8	0.8
V	46.6	Fermi II	-35.5	-16.0	151.3	-11.4	13.0	-1.1	-1.9	-13.0	3.7	19.7	-0.6	-2.0	2.5	1.0

Table XV. spdf Solutions to π^+-p and π^--p DCS, polarization, total cross section, and π^--p $\rightarrow \pi^0$n DCS.

$M_{expected} = 52$[a]

	M	$S_{3,1}$	$P_{3,1}$	$P_{3,3}$	$D_{3,3}$	$D_{3,5}$	$F_{3,5}$	$F_{3,7}$	$S_{1,1}$	$P_{1,1}$	$P_{1,3}$	$D_{1,3}$	$D_{1,5}$	$F_{1,5}$	$F_{1,7}$
I	43.7	-14.4	1.1	135.1	5.4	-6.9	0.8	-2.0	-6.0	-5.8	1.5	-5.7	15.8	-0.2	2.5
II	64.2	-21.2	-12.1	137.2	-3.3	1.5	-1.8	3.3	10.9	23.1	-3.5	6.5	0.6	2.1	-1.2
III	71.7	-15.6	-0.7	135.3	4.2	-6.0	0.7	-1.3	5.0	27.9	9.2	-0.5	-0.7	-3.2	-0.5

[a] $M_{expected}$ means the number of degrees of freedom, i.e., (number of experimental points fitted) minus (number of phase shifts varied).

Solution (2)—Although the search yielding this solution began with the $I = 3/2$ phase shifts being fixed at the Fermi I values, the final solution demonstrates a definite Fermi II behavior (i.e., $D_{3,3} - D_{3,5} < 0$). The $I = 3/2$ phase shifts are very different from the Fermi II solution of Foote, but the fit to the π^+-p data is nevertheless quite good. The π^--p polarization data is fitted rather badly, as seen from Fig. 10; however, the fit to the remaining data is sufficiently good that the large contribution to M of the π^--p polarization data (≈ 10) is insufficient to rule out the solution.

Solution (3)—This is a somewhat poorer fit to the data, but still does not possess a sufficiently high M value to be ruled out. The $I = 3/2$ phase shifts are of the Fermi I type, but are not nearly as consistent with the Foote solution as are those of solution (1). Each phase shift does, however, lie within the quoted uncertainty of the Foote solution.

It should be noted that, although the Fermi II solution was used as a starting point for 200 random sets, it was not possible to find any solution that adequately fitted all the π-p data. Thus it can be concluded that Foote's solution of Fermi II can not be used to fit π^--p and π^+-p data simultaneously.

Other $I = 3/2$ starting points. As in the case of the spd analyses, a limited amount of searching was done in which the less-likely $I = 3/2$ solutions (See Table VI, Foote[3]) were used as starting points. The two solutions treated were the Yang II set and solution No. 6, which is unnamed in the above reference (Foote) and so is here referred to as Fermi Ia. About 100 random cases were examined, with no satisfactory solutions to π^+-p and π^--p (DCS and polarization) appearing.

3. Error Analysis

The matrix-inversion error routine described in Sec. IV.B was applied to the spd solution as well as the three spdf solutions. The errors are quoted, as well as a brief summary of the effects of various data on these errors.

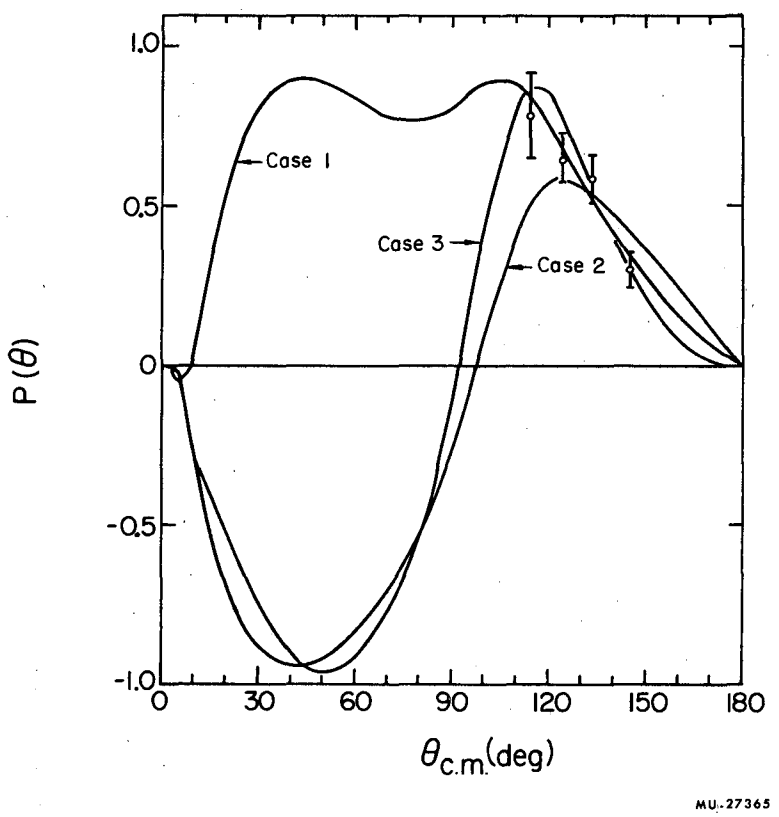

Fig. 10. Recoil-proton polarization in π^--p elastic scattering at 310 MeV. Cases plotted are those given in Table XV.

Error matrices. The error matrices for the four solutions discussed above are tabulated in Appendix B. It is seen that in the spd solution, all rms errors are from 0.5 to 1 deg. The correlation coefficients are all relatively small. For the spdf solutions, the errors are considerably larger, and the correlation coefficients have also increased in size. The quoted errors on the $I = 3/2$ phase shift are seen to be similar to those quoted by Foote,[3] indicating that the inclusion of π^--p data has a negligible effect on the $I = 3/2$ phase-shift error.

Effect of various data on errors. The spd solution was examined in an effort to determine what types of information was most effective in reducing the uncertainties on the phase shift. Table XVI gives the rms errors on all the phase shifts when various combinations of data are included.

4. Inelastic parameters.

To determine the effect of inelastic parameters on the phase shifts, an inelastic total cross section of $\sigma_I = 1.5 \pm 0.8$ mb[20] was included in the search program, and the inelastic parameters allowed to vary. Only the four final solutions were examined; the results are given in Table XVII. In all cases, the inelastic parameters were started at 1.0, although starting them at 0.95 and 0.90 yielded essentially the same results.

Table XVI. Effect of various data on phase-shift errors (spd solution).

All cases include the following π^+-p data: 23 DCS points, 4 polarization points (Pol), and 1 total cross section. In addition, the following π^--p data	Errors (in deg) on I = 1/2 phase shifts				
	$S_{1,1}$	$P_{1,1}$	$P_{1,3}$	$D_{1,3}$	$D_{1,5}$
28 DCS	0.9	0.5	1.3	0.3	0.9
28 DCS, 1 TCS	0.8	0.4	1.0	0.3	0.6
28 DCS, 1 TCS, 4 Pol	0.7	0.4	0.9	0.3	0.6
7 DCS,[a] 1 TCS, 4 Pol	0.8	0.5	1.2	0.4	0.8
7 DCS,[a] 1 TCS, 4 Pol, 5 charge-exchange DCS coefficients	0.8	0.5	1.1	0.3	0.7
28 DCS, 1 TCS, 4 Pol, 5 charge-exchange DCS coefficients	0.6	0.4	0.9	0.3	0.6

[a]The 7 DCS points are distributed evenly throughout the angular region.

Table XVII. spd and spdf solutions including the inelastic total cross section.

	spd solution						
	$S_{3,1}$	$P_{3,1}$	$P_{3,3}$	$D_{3,3}$	$D_{3,5}$		
I = 3/2 phase shifts	-18.9	-5.0	135.5	1.6	-3.4		
	$S_{1,1}$	$P_{1,1}$	$P_{1,3}$	$D_{1,3}$	$D_{1,5}$		
I = 1/2 phase shifts	-6.0	-3.9	4.0	-5.3	14.9		
Corresponding inelastic parameters[a]	0.98	1.00	1.00	0.99	1.00		
	spdf solution I						
	$S_{3,1}$	$P_{3,1}$	$P_{3,3}$	$D_{3,3}$	$D_{3,5}$	$F_{3,5}$	$F_{3,7}$
I = 3/2 phase shifts	-14.9	0.4	135.1	5.1	-6.5	0.8	-1.8
	$S_{1,1}$	$P_{1,1}$	$P_{1,3}$	$D_{1,3}$	$D_{1,5}$	$F_{1,5}$	$F_{1,7}$
I = 1/2 phase shifts	-5.9	-5.5	1.7	-5.5	15.3	-0.1	2.3
Corresponding inelastic parameters	1.00	1.00	0.99	0.99	1.00	1.00	1.00
	spdf solution II						
	$S_{3,1}$	$P_{3,1}$	$P_{3,3}$	$D_{3,3}$	$D_{3,5}$	$F_{3,5}$	$F_{3,7}$
I = 3/2 phase shifts	-21.1	-11.8	137.0	-3.1	1.2	-1.7	3.1
	$S_{1,1}$	$P_{1,1}$	$P_{1,3}$	$D_{1,3}$	$D_{1,5}$	$F_{1,5}$	$F_{1,7}$
I = 1/2 phase shifts	10.9	23.0	-3.6	5.9	0.3	1.8	-0.7
Corresponding inelastic parameters	1.00	0.94	1.00	1.00	1.00	1.00	1.00

Table XVII. spd and spdf solutions including the inelastic total cross section. (continued)

	spdf solution III						
	$S_{3,1}$	$P_{3,1}$	$P_{3,3}$	$D_{3,3}$	$D_{3,5}$	$F_{3,5}$	$F_{3,7}$
I = 3/2 phase shifts	-15.4	-0.4	135.6	4.4	-6.2	0.7	-1.4
	$S_{1,1}$	$P_{1,1}$	$P_{1,3}$	$D_{1,3}$	$D_{1,5}$	$F_{1,5}$	$F_{1,7}$
I = 1/2 phase shifts	3.7	26.4	8.6	-0.3	3.1	-0.6	-0.1
Corresponding inelastic parameters	1.00	1.00	0.98	1.00	1.00	1.00	1.00

[a] See Sec. II.B.1.

V. DISCUSSION OF RESULTS

A. General

The work described above has apparently fallen somewhat short of its goal, i.e., the complete and unambiguous determination of the $I = 1/2$ pions nucleon phase shifts at this energy. Although the situation seems otherwise reasonably well resolved in the spd analysis, inclusion of f waves complicates matters considerably.

Perhaps the most disturbing aspect of the spdf wave analysis is the fact that, although the f waves are small in all the satisfactory solutions, the presence of even these very small f waves is seen to radically change the magnitude, and in some cases also the sign, of the phase shifts of the lower orbital-angular-momentum states. This casts doubt on the very premise on which phase-shift analysis is based, i.e., that one can approximate the infinite series that represents the scattering amplitudes by the first few terms. It seems to indicate that the remaining terms in the expansion, although minute in themselves, can nevertheless exert a considerable influence on the larger terms.

A major limitation of the data that now exist at 310 MeV is the very limited angular region of thepolarization data, both in π^+-p and π^--p. Especially in π^--p, it would be very instructive to push toward smaller c.m. angles in an attempt to determine the value of polarization at θ near 90 deg. As was mentioned in Sec. III.B1., the analyzing power of carbon drops sharply below about 110 MeV, so that it might still be possible to measure a point at θ_{cm} of about 100 deg, which would certainly be of some value.

In the energy region corresponding to θ_{cm} = 30 to 60 deg, helium is an effective analyzer; some attempts have been made to measure polarization of the recoil proton in this region but no data exist at present. A recent preliminary experiment by Booth[21] indicates also the possibility of measuring recoil-neutron polarization in the reaction $\pi^- + p \rightarrow \pi^0 + n$; this measurement, also in the 30 to 60 deg region, would be useful as well in resolving ambiguities between solutions.

Developments in polarized targets may in the future make it possible to measure additional quantities corresponding to the triple-scattering parameters in nucleon-nucleon scattering (Ypsilantis)[17]. This would give information on $Im(g^{*}h)$ and hence yield another independent experimental quantity.

B. Comparison with Theoretical Predictions

Relativistic dispersion relations have been used by Chew, Goldberger, Low, and Nambu to derive equations for low-energy s-, p-, and d-wave pion-nucleon scattering.[22] It is assumed in this work that the (3/2, 3/2) resonance dominates the dispersion integrals, and the pion-pion interaction has been neglected. This work has been ex-extended by Bowcock et al. to make f-wave phase-shift predictions.[23] These predictions are summarized and compared to the aforementioned solutions in the following subsections.

1. p Waves

The p-wave predictions and the corresponding p-wave phase shifts of the four satisfactory solutions are given in Table XVIII. In general, the spd solution shows satisfactory agreement in the I = 3/2 shifts. The spdf solutions show somewhat poorer agreement, but it is still not unreasonable. The I = 1/2 shifts, however, are in complete disagreement for all four solutions. In fact, none of the solutions encountered during the various stages of analysis display the behavior predicted by Chew et al.[22]

2. d Waves

Table XIX lists the predictions for d waves and the corresponding phase shifts. Again, the spd solution shows the best agreement with I = 3/2 shifts, while spdf I and spdf III at least display the predicted sign. Solution spdf II (which has Fermi II behavior, as pointed out in Sec. IV.B.2) disagrees in sign. Again, there is very poor agreement in the I = 1/2 phase shifts. Only solution spdf III could be considered to have satisfactory agreement with all four d-wave phase shifts ; this solution disagrees badly in p-wave phase shifts (see above).

Table XVIII. Comparison of solutions with dispersion-relation predictions of Chew, Goldberger, Low, and Nambu,[a] for p-wave agreement.

Solution	$P_{3,1}$	$P_{3,3}$	$P_{1,1}$	$P_{1,3}$
Prediction of Chew et al.	-5.0	124.2	-19.5	-5.0
spd	-4.9± 0.5	135.5± 0.6	-4.0± 0.4	3.9± 0.9
spdf I	1.1± 2.0	135.1± 0.6	-5.8± 0.8	1.5± 1.3
spdf II	-12.2± 0.9	137.2± 0.8	23.1± 0.9	-3.5± 0.7
spdf III	-0.7± 1.7	135.3± 0.6	27.9± 1.3	9.2± 1.0

[a]See reference 22.

Table XIX. Comparison of solutions with dispersion-relation predictions of Chew, Goldberger, Low, and Nambu,[a] for d-wave agreement.

Solution	$D_{3,3}$	$D_{3,5}$	$D_{1,3}$	$D_{1,5}$
Prediction of Chew et al.	.3°	-2.5°	-1.5°	.9°
spd	1.7± 0.3	-3.6± 0.4	-5.5± .3	15.2± .6
spdf I	5.4± 1.0	-6.9± 1.0	-5.7± .4	15.8± 0.8
spdf II	-3.3± 0.6	1.5± 0.8	6.5± 0.5	0.6± 0.5
spdf III	4.2± 1.0	-6.0± 0.9	-0.5± 0.8	-0.7± 0.6

[a]See reference 22.

3. f Waves

Bowcock, Cottingham, and Lurie have predicted f-wave phase shifts at this energy to be less than 0.2 deg.[23] This is not within the experimental errors quoted on the f-wave phase shifts (see Appendix B). Much more accurate determination of f waves would be necessary to make meaningful comparisons here.

C. Conclusions

The phase-shift solutions discussed in this report, however ambiguous, are probably still meaningful in making comparisons with predicted values. The fact that no solution even approximately agreeing with the predictions of dispersion relations appears in this phase-shift analysis tends to cast some doubt on the ability of dispersion relations to predict phase shifts, and perhaps on the validity of phase-shift analysis as a whole. More data are certainly needed, both to resolve present ambiguities and also to make the phase-shift solutions more restrictive.

Of some value is the rather strong evidence against the Fermi II $I = 3/2$ solution of Foote.[3] Although another solution of the Fermi II type did appear, Foote's particular solution must be regarded as very unlikely.

Although this analysis cannot be regarded as complete, it is hoped that the addition of further data will clarify the problems and perhaps produce a single phase-shift solution. It is hoped that this paper represents a significant contribution toward the quantitative understanding of the pion-nucleon interaction.

Acknowledgments

It is a pleasure to acknowledge the invaluable assistance of Dr. James H. Foote, who first aroused my interest in polarization measurements during my first year at the Lawrence Radiation Laboratory. His willing contributions to both the experimental work and the subsequent analysis, together with enlightening discussions and counsel, have aided immeasurably in the completion of this project.

The continued support of Professor Emilio Segrè, together with the contributions of the entire research group under his leadership, is gratefully recognized.

To my able coworker Dr. Hugo R. Rugge goes a debt of gratitude for his unselfish devotion to all phases of experiment and analysis. His careful measurement of cross sections made possible the phase-shift analysis described herein, and his willingness and co-operation throughout the project is deeply appreciated.

Dr. Norman E. Booth has contributed valuable experience to the experimental work, as well as helpful advice throughout.

Dr. Thomas Ypsilantis has lent enthusiastic support and optimism, and the many suggestions of Dr. Herbert M. Steiner have been most helpful. Dr. Ernest H. Rogers is acknowledged for innumerable informative discussions on a variety of topics. Mr. David Jenkins has ably assisted in much of the tedious programming and computation.

The fine co-operation of Mr. James T. Vale and Mr. Lloyd B. Houser of the 184-inch synchrocyclotron, as well as the efficient work of the cyclotron crew, was of great importance to the success of the experiment, as was the efficient setup work of Mr. Robert E. Walton and the accelerator technicians.

This work was done under the auspices of the U. S. Atomic Energy Commission.

APPENDICES

A. Additional Equations Used in PIPANAL

As mentioned in Sec. IV.B, a certain calculated value of the inelastic cross section is added to the integrated value of the DCS, and the result is compared to a measured value for the total cross section. In this appendix the equations for the inelastic cross section are listed.

1. π^+-p inelastic cross section

Here we have $\sigma(\text{elastic}) + \sigma(\text{inelastic}) = \sigma(\text{total})$.
The $\sigma(\text{elastic})$ is obtained by integrating the elastic DCS, from which we have

$$\sigma(\text{elastic}) = \pi \lambda^2 \sum_{\ell=0}^{\ell_{max}} \left\{ (\ell+1)\left[1 + (\rho_\ell^+)^2 - 2\rho_\ell^+ \cos 2\alpha_\ell^+\right] + \ell\left[1 + (\rho_\ell^-)^2 - 2\rho_\ell^+ \cos 2\alpha_\ell^-\right]\right\} . \tag{A.1}$$

The quantity $\sigma(\text{total})$ is related through the Optical Theorem to the imaginary part of the forward scattering amplitude by $\sigma(\text{total}) = 4\pi\lambda \operatorname{Im} f(\theta = 0 \text{ deg})$. At $\theta = 0$ deg, all the Legendre functions are unity, while the associate Legendre functions are zero. Hence

$$f(\theta = 0 \text{ deg}) = \frac{\lambda}{2} \sum_{\ell=0}^{\ell_{max}} (\ell+1)\left[1 - \rho_\ell^+ \cos 2\alpha_\ell^+\right] + \ell\left[1 - \rho_\ell^- \cos 2\alpha_\ell^-\right] . \tag{A.2}$$

Subtracting $\sigma(\text{elastic})$ from $\sigma(\text{total})$, we have

$$\sigma(\text{inelastic}) = \pi\lambda^2 \sum_{\ell} (\ell+1)\left[1 - (\rho_\ell^+)^2\right] + \ell\left[1 - (\rho_\ell^-)^2\right] . \tag{A.3}$$

2. π^--p inelastic cross section

The same method as above is employed to obtain the inelastic cross section for π^--p scattering. However, in this case, we must consider as elastic scattering both direct and charge-exchange scattering:

$$\sigma(\text{total}) = \sigma(\text{direct}) + \sigma(\text{charge-exchange}) + \sigma(\text{inelastic}).$$

The final result for σ(inelastic) is

$$\sigma(\text{inelastic}) = \pi \lambda\!\!\!^{-2} \sum_{\ell} (\ell+1) \left[1 - \frac{1}{3} (\rho_\ell^+)^2 - \frac{2}{3} \eta_\ell^{+2}\right] + \ell \left[1 - \frac{1}{3} (\rho_\ell^-)^2 - \frac{2}{3} (\eta_\ell^-)^2\right]. \tag{A.4}$$

These inelastic cross sections are calculated over the entire solid angle, so a small correction must be made to them in order to use them in conjunction with cutoff angles. In our case this correction was $< 2\%$ of the inelastic cross section.

B. Error Routine Discussion and Error Matrices

This appendix explains the manner in which PIPANAL 1CF4 calculates the partial derivatives necessary for the error routine outlined in Sec. IV.B. The use of the error matrix in computing errors in functions of phase shifts is outlined. Finally, the error matrices for the four phase-shift solutions are presented.

1. Calculation of Partial Derivatives

The value of M in the neighborhood of the minimum M_0 can be given by a Taylor expansion:

$$M(\delta_1 + \Delta\delta_1,\ \delta_2 + \Delta\delta_2,\ \ldots,\ \delta_n + \Delta\delta_n) = M_0 + \sum_{i=1}^{n} \frac{\partial M}{\partial \delta_i} \Delta\delta_i$$

$$+ \frac{1}{2} \sum_{i=1}^{n} \sum_{j=1}^{n} \frac{\partial^2 M}{\partial \delta_i \, \partial \delta_j} \Delta\delta_i \, \Delta\delta_j + (\text{higher-order terms}),$$

where $\delta_1 \cdots \delta_n$ are the values of the phase shifts at the minimum, $M_0 = M(\delta_1 \cdots \delta_n)$, and all derivatives are evaluated at the minimum. At the minimum, however, all the $\partial M/\partial \delta_i = 0$, so,

$$\Delta M = M(\delta_1 + \Delta\delta_1,\ \delta_2 + \Delta\delta_2,\ \cdots,\ \delta_n + \Delta\delta_n) - M_0$$

$$\approx \frac{1}{2} \sum_{i=1}^{n} \sum_{j=1}^{n} \frac{\partial^2 M}{\partial \delta_i \partial \delta_j} \Delta\delta_i \Delta\delta_j .$$

Varying only one phase shift yields the equation

$$\Delta M_i^{+} = M(\delta_1,\ \delta_2 \cdots \delta_i + \Delta\delta_i \cdots \delta_n) - M_0 = \frac{1}{2} \frac{\partial^2 M}{\partial \delta_i^2} (\Delta\delta_i)^2 .$$

Since the region around the minimum may not be entirely symmetrical, the program computes ΔM by varying δ_i in both directions, and the average value of the partial derivative is used:

$$\frac{\partial^2 M}{\partial \delta_i^2} = \frac{\Delta M_i^{+} + \Delta M_i^{-}}{(\Delta\delta_i)^2} .$$

When two phase shifts are varied simultaneously, the following form is obtained:

$$\Delta M_{ij}^{++} = M(\delta_1,\ \delta_2,\ \cdots,\ \delta_i + \Delta\delta_j,\ \cdots,\ \delta_k + \Delta\delta_k,\ \cdots \delta_n)$$

$$- M_0 = \frac{1}{2} \frac{\partial^2 M}{\partial \delta_i \partial \delta_j} \Delta\delta_i \Delta\delta_j .$$

In this case, there are four different combinations of changes corresponding to $\delta_i \pm \Delta\delta_i$ and $\delta_j \pm \Delta\delta_j$. The average is then taken over these four quantities, yielding

$$\frac{\partial^2 M}{\partial \delta_i \partial \delta_j} = \frac{\Delta M_{ij}^{++} + \Delta M_{ij}^{--} - \Delta M_{ij}^{+-} - \Delta M_{ij}^{-+}}{4\,|\,\Delta\delta_i \Delta\delta_j\,|} .$$

The partial derivatives thus calculated form the matrix defined by

$$G_{ij} = \frac{1}{2} \frac{\partial^2 M}{\partial \delta_i \partial \delta_j} .$$

2. Use of the Error Matrix

The inverse of the G matrix is the so-called error matrix G^{-1}, whose elements have the properties[22]

$$G^{-1}_{ii} = (\Delta\delta_i)_{rms} , \text{ and } G^{-1}_{ij} = C_{ij} (\Delta\delta_i)_{rms} (\Delta\delta_j)_{rms},$$

where C_{ij} is the correlation coefficient, which is a measure of the interdependence of δ_i and δ_j.

In order to calculate the rms error in a function F of the phase shifts δ, the following expression is used:[25]

$$(\Delta F)_{rms} = \sqrt{\sum_{i=1}^{n} \sum_{j=1}^{n} \frac{\partial F}{\partial \delta_i} \frac{\partial F}{\partial \delta_j} (G^{-1})_{ij}} .$$

3. Error Matrices for the Aforementioned Solutions

Tables BI through BIV present the error matrices corresponding to the spd solution and the three spdf solutions discussed in Sec. III.B. All elements are expressed in degrees squared.

Table B I. Error matrix for spd solution (expressed in deg^2).

	$S_{3,1}$	$P_{3,1}$	$P_{3,3}$	$D_{3,3}$	$D_{3,5}$	$S_{1,1}$	$P_{1,1}$	$P_{1,3}$	$D_{1,3}$	$D_{1,5}$
$S_{3,1}$	0.4	0.2	0.2	0.1	-0.2	-0.2	-0.2	-0.0	-0.1	0.1
$P_{3,1}$		0.3	0.1	0.1	-0.2	-0.1	-0.2	-0.0	-0.0	0.1
$P_{3,3}$			0.4	0.0	0.0	0.0	-0.1	0.2	-0.1	0.2
$D_{3,3}$				0.1	-0.1	-0.1	-0.0	-0.0	-0.0	0.0
$D_{3,5}$					0.2	0.1	0.1	0.1	0.0	-0.0
$S_{1,1}$						0.4	0.0	0.5	0.0	0.1
$P_{1,1}$							0.2	-0.1	0.1	-0.2
$P_{1,3}$								0.8	-0.1	0.3
$D_{1,3}$									0.1	-0.1
$D_{1,5}$										0.4

Table B II. Error matrix for spdf solution I (expressed in deg^2).

	$S_{3,1}$	$P_{3,1}$	$P_{3,3}$	$D_{3,3}$	$D_{3,5}$	$F_{3,5}$	$F_{3,7}$	$S_{1,1}$	$P_{1,1}$	$P_{1,3}$	$D_{1,3}$	$D_{1,5}$	$F_{1,5}$	$F_{1,7}$
$S_{3,1}$	3.2	3.3	0.5	1.5	-1.7	-0.0	-0.9	-1.5	-1.3	-1.5	-0.2	-0.1	0.0	0.7
$P_{3,1}$		3.8	0.4	1.8	-1.9	-0.0	-1.1	-1.7	-1.4	-1.7	-0.2	-0.3	0.1	0.8
$P_{3,3}$			0.4	0.1	-0.1	0.0	-0.1	-0.2	-0.3	-0.0	-0.1	0.2	0.0	0.1
$D_{3,3}$				0.9	-0.9	0.0	-0.5	-0.8	-0.6	-0.8	-0.1	-0.2	0.0	0.3
$D_{3,5}$					1.0	0.0	0.5	0.9	0.7	0.9	0.1	0.2	-0.0	-0.4
$F_{3,5}$						0.1	-0.0	-0.0	-0.0	-0.0	-0.0	-0.0	-0.0	-0.0
$F_{3,7}$							0.3	0.5	0.4	0.5	0.1	0.1	-0.0	-0.2
$S_{1,1}$								2.2	0.6	1.3	0.3	0.5	-0.2	0.3
$P_{1,1}$									0.7	0.5	0.2	-0.1	0.0	-0.3
$P_{1,3}$										1.7	-0.0	0.6	-0.0	-0.3
$D_{1,3}$											0.1	-0.1	-0.0	0.1
$D_{1,5}$												0.6	-0.0	0.1
$F_{1,5}$													0.1	-0.1
$F_{1,7}$														0.5

Table B III. Error matrix for spdf solution II (expressed in deg^2.)

	$S_{3,1}$	$P_{3,1}$	$P_{3,3}$	$D_{3,3}$	$D_{3,5}$	$F_{3,5}$	$F_{3,7}$	$S_{1,1}$	$P_{1,1}$	$P_{1,3}$	$D_{1,3}$	$D_{1,5}$	$F_{1,5}$	$F_{1,7}$
$S_{3,1}$	0.2	0.1	0.1	0.1	-0.1	0.0	-0.0	0.2	0.1	0.0	0.0	0.0	-0.0	-0.0
$P_{3,1}$		0.7	-0.4	0.5	-0.6	0.3	-0.3	0.2	-0.2	0.2	-0.2	0.3	-0.1	0.1
$P_{3,3}$			0.7	-0.3	0.5	-0.2	0.2	0.2	0.4	-0.1	0.2	-0.2	0.1	-0.1
$D_{3,3}$				0.4	-0.4	0.2	-0.2	0.1	-0.1	0.1	-0.2	0.2	-0.1	0.1
$D_{3,5}$					0.6	-0.2	0.3	-0.1	0.1	-0.1	0.2	-0.3	0.1	-0.1
$F_{3,5}$						0.2	-0.1	0.1	-0.1	0.1	-0.1	0.1	-0.1	0.1
$F_{3,7}$							0.2	-0.1	0.1	-0.1	0.1	-0.1	0.1	-0.1
$S_{1,1}$								1.8	0.7	0.4	0.1	0.1	-0.1	0.1
$P_{1,1}$									0.9	0.1	0.3	0.1	0.1	-0.0
$P_{1,3}$										0.5	0.0	0.2	-0.0	0.1
$D_{1,3}$											0.2	-0.0	0.1	-0.0
$D_{1,5}$												0.3	-0.2	0.1
$F_{1,5}$													0.1	-0.1
$F_{1,7}$														0.1

Table B IV. Error matrix for spdf solution III (expressed in deg^2).

	$S_{3,1}$	$P_{3,1}$	$P_{3,3}$	$D_{3,3}$	$D_{3,5}$	$F_{3,5}$	$F_{3,7}$	$S_{1,1}$	$P_{1,1}$	$P_{1,3}$	$D_{1,3}$	$D_{1,5}$	$F_{1,5}$	$F_{1,7}$
$S_{3,1}$	1.9	2.2	0.2	1.2	-1.1	0.2	-0.7	0.4	-0.7	0.8	-0.6	0.6	-0.1	0.4
$P_{3,1}$		3.0	0.1	1.7	-1.4	0.2	-0.9	0.4	-1.1	1.1	-0.8	0.7	-0.1	0.6
$P_{3,3}$			0.4	0.0	0.0	0.0	-0.0	0.2	0.3	0.2	-0.0	0.0	0.0	0.0
$D_{3,3}$				1.1	-0.8	0.1	-0.6	0.2	-0.7	0.6	-0.5	0.4	-0.1	0.3
$D_{3,5}$					0.8	-0.1	0.4	-0.2	0.6	-0.5	0.4	-0.4	0.1	-0.3
$F_{3,5}$						0.1	-0.1	0.0	-0.1	0.1	0.1	0.0	-0.0	0.0
$F_{3,7}$							0.3	-0.1	0.4	-0.3	0.2	-0.2	0.0	-0.2
$S_{1,1}$								1.9	0.2	1.0	-0.7	0.4	-0.4	0.0
$P_{1,1}$									1.6	-0.6	0.4	-0.3	0.2	-0.2
$P_{1,3}$										1.0	-0.5	0.5	-0.3	0.2
$D_{1,3}$											0.6	-0.2	0.1	-0.1
$D_{1,5}$												0.3	-0.1	0.2
$F_{1,5}$													0.2	0.0
$F_{1,7}$														0.1

REFERENCES

1. J. Foote, O. Chamberlain, E. Rogers, H. Steiner, C. Wiegand, and T. Ypsilantis, Phys. Rev. 122, 948 (1961).
2. E. H. Rogers, O. Chamberlain, J. Foote, H. Steiner, C. Wiegand, and T. Ypsilantis, Revs. Modern Phys. 33, 356 (1961).
3. J. Foote, O. Chamberlain, E. Rogers, and H. Steiner, Phys. Rev. 122, 959 (1961).
4. V. Zinov, A. Konin, S. Korenchenko, and B. Pontecorvo, Soviet Phys. JETP 11, 1233 (1960).
5. I. Vasilevskii and V. Vishnyakov, Soviet Phys. JETP 11, 323 (1960).
6. Hugo R. Rugge (Lawrence Radiation Laboratory), private communication.
7. H. A. Bethe and P. Morrison, Elementary Nuclear Theory, 2nd Edition (John Wiley & Sons, Inc., New York, 1956), pp. 133-142.
8. J. Ashkin, Suppl. Nuovo Cimento 14, 221 (1959).
9. H. A. Bethe and F. de Hoffmann, Mesons and Fields, (Row, Peterson and Company, Evanston, Illinois, 1955), Vol. II.
10. H. P. Stapp, T. J. Ypsilantis, and N. Metropolis, Phys. Rev. 105, 302 (1957).
11. Frank T. Solmitz, Phys. Rev. 94, 1799 (1954).
12. C. L. Critchfield and D. C. Dodder, Phys. Rev. 76, 602 (1949).
13. William A. Wenzel, Millimicrosecond Coincidence Circuit for High-Speed Counting, University of California Radiation Laboratory Report UCRL-8000, October 1957 (unpublished).
14. J. M. Dickson and D. C. Salter, Nuovo Cimento 6, 235 (1957).
15. H. Tyren and Th. A. J. Maris, Nuclear Phys. 4, 637 (1957); P. Hillman, A. Johansson, and H. Tyren, Nuclear Phys. 4, 648 (1957); Th. A. J. Maris and H. Tyren, Nuclear Phys. 4, 662 (1957); R. Alphonce, A. Johansson, and G. Tibell, Nuclear Phys. 4, 672 (1957).
16. E. M. Hafner, Phys. Rev. 111, 297 (1958).

17. Tom J. Ypsilantis, Experiments on Polarization in Nucleon-Nucleon Scattering at 310 MeV, University of California Radiation Laboratory Report (thesis), UCRL-3047, June 1955 (unpublished).

18. H. L. Anderson, E. Fermi, R. Martin, and D. E. Nagle, Phys. Rev. 91, 155 (1953).

19. John C. Caris, Charge-Exchange Scattering of Negative Pions by Hydrogen at 230, 260, 290, 317, and 371 MeV (thesis), Lawrence Radiation Laboratory Report UCRL-9048, March 1960 (unpublished).

20. B. C. Barish, Richard Kurz, and Julius Solomon (Lawrence Radiation Laboratory), private communication.

21. Norman E. Booth (Lawrence Radiation Laboratory), private communication.

22. G. F. Chew, M. L. Goldberger, F. E. Low, and Y. Nambu, Phys. Rev. 106, 1337 (1957).

23. J. Bowcock, W. N. Cottingham, and D. Lurié, Nuovo Cimento 16, 918 (1960).

24. H. Anderson, W. Davidon, M. Glicksman, and U. Kruse, Phys. Rev. 100, 279 (1955).

25. H. Anderson and W. Davidon, Nuovo Cimento 5, 1238 (1957).

LEGAL NOTICE

This report was prepared as an account of Government sponsored work. Neither the United States, nor the Commission, nor any person acting on behalf of the Commission:

A. Makes any warranty or representation, expressed or implied, with respect to the accuracy, completeness, or usefulness of the information contained in this report, or that the use of any information, apparatus, method, or process disclosed in this report may not infringe privately owned rights; or

B. Assumes any liabilities with respect to the use of, or for damages resulting from the use of any information, apparatus, method or process disclosed in this report.

As used in the above, "person acting on behalf of the Commission" includes any employee or contractor of the commission, or employee of such contractor, to the extent that such employee or contractor of the Commission, or employee of such contractor prepares, disseminates, or provides access to, any information pursuant to his employment or contract with the Commission, or his employment with such contractor.